BioTube: Designing and Fabricating Biodegradable Hollow Tubular Devices Through Progressive Crosslinking Alginate

Yuecheng Peng*
Mechanical Engineering, Morphing Matter Lab
University of California, Berkeley
Berkeley, California, USA
University of Washington
Seattle, Washington, USA
ychpeng@uw.edu

Mako Miyatake*
Mechanical Engineering, Morphing Matter Lab
University of California, Berkeley
Berkeley, California, USA
mako_miyatake@berkeley.edu

Tyler L Peng
Mechanical Engineering, Morphing Matter Lab
University of California, Berkeley
Berkeley, California, USA
tyler.peng@berkeley.edu

Qiuyu Lu
Mechanical Engineering, Morphing Matter Lab
University of California, Berkeley
Berkeley, California, USA
qiuyulu@berkeley.edu

Yue Yang
Mechanical Engineering, Morphing Matter Lab
University of California, Berkeley
Berkeley, California, USA
yang_yue@zju.edu.cn

Lining Yao
Mechanical Engineering, Morphing Matter Lab
University of California, Berkeley
Berkeley, California, USA
liningy@berkeley.edu

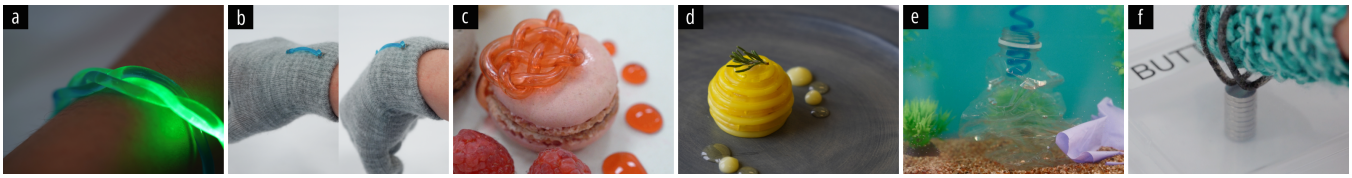

Figure 1: Examples of BioTube applications: (a) Interactive glowing bracelet with displacement-sensing capabilities. (b) Temporary stretch-sensing augmentation of gloves for gamified wrist rehabilitation exercises. (c) Pneumatic shape-changing dessert with a "pumping heart." (d) Dessert featuring spatially mixed dual flavors. (e) Underwater biodegradable gripper for collecting plastic waste, for example, water bottles. (f) Magnetic elastomer fiber cast using hollow tubular alginate as a sacrificial template, which can be integrated into textiles for haptic feedback.

Abstract

We present **BioTube**, a sustainable and highly accessible DIY fabrication approach for creating hollow tubular alginate, and demonstrate its potential for making biodegradable transient devices. This technique involves extruding alginate into a calcium solution, initiating a progressive crosslinking process that starts from the outer shell and progresses inward. This controlled process removes the uncrosslinked core before complete gelation, yielding hollow alginate fibers. To further enhance the capabilities of BioTube, we explored three further crosslinking strategies to customize the fiber shape, local cross-sectional geometry, and stiffness. The versatility of this method is demonstrated through three key functional primitives: shape, morphing, and sensing. These capabilities are further illustrated through five application examples, including transient wearables, edible shape-changing interfaces, experimental gastronomy, underwater grippers, and sacrificial casting molds. We believe that BioTube will expand the design possibilities for alginate, enabling the creation of innovative biodegradable devices.

CCS Concepts

• **Human-centered computing** → **Interactive systems and tools**.

Keywords

Biomaterials, hydrogels, Bio-HCI, bio-design, sustainability

*authors contributed equally

This work is licensed under a Creative Commons Attribution-NonCommercial-ShareAlike International 4.0 License.

CHI '25, Yokohama, Japan

© 2025 Copyright held by the owner/author(s).

ACM ISBN 979-8-4007-1394-1/25/04
https://doi.org/10.1145/3706598.3714165

ACM Reference Format:
Yuecheng Peng, Mako Miyatake, Tyler L Peng, Qiuyu Lu, Yue Yang, and Lining Yao. 2025. BioTube: Designing and Fabricating Biodegradable Hollow Tubular Devices Through Progressive Crosslinking Alginate. In *CHI Conference on Human Factors in Computing Systems (CHI '25), April 26–May 01, 2025, Yokohama, Japan.* ACM, New York, NY, USA, 21 pages. https://doi.org/10.1145/3706598.3714165

1 Introduction

The growing interest in sustainable design within the Human-Computer Interaction (HCI) community has led researchers and designers to explore biodegradable materials, such as different naturally derived hydrogels [43, 46, 47, 70, 80, 121], mycelium [100], food waste [5], and coffee grounds [79], for creating various devices. In this work, we focus on one biodegradable material, alginate—a natural polysaccharide-based hydrogel known for its abundant availability, low cost, excellent biocompatibility, and biodegradability [93]. The fabrication of alginate hydrogels typically involves crosslinking, a process where calcium ions (Ca^{2+}) induce the formation of a gel by linking the polymer chains together, resulting in a solid structure [40, 73].

Various forms of alginate have been explored, including films [43, 70], pastes [43], fibers [97, 121], molded parts [70], and 3D-printed free-form geometries [92]. Among these, hollow tubular structures represent a particularly promising area due to their applications in actuators [38, 42], high-sensitivity sensors [22], and dynamic displays [54], etc. However, fabricating such structures using alginate has been challenging. The process typically requires complex coaxial devices [13, 64, 69, 117] or intricate template-making techniques [72, 90, 106], which can be cumbersome and often inaccessible to DIY and maker communities.

To address these challenges, we introduce BioTube, a DIY-friendly fabrication approach for creating hollow tubular alginate structures. Central to our method is the concept of progressive crosslinking, where calcium ions (Ca^{2+}) gradually diffuse into the alginate fiber from the outer surface toward the center, progressively inducing crosslinking as they move inward. This progressive process allows for control over the wall thickness by adjusting the crosslinking time. Before gelation is complete, the alginate fiber is taken out of the calcium bath and rinsed with water, allowing the uncrosslinked core to be removed, resulting in a hollow fiber. This time-dependent crosslinking allows reshaping during gelation, enabling the fiber to retain new shapes through mold-assisted crosslinking or to modify its cross-sectional geometry through asymmetric crosslinking. Additionally, we can tune the stiffness of the fibers by immersing them in a more concentrated calcium solution. Moreover, a post-treatment process can be used to extend the longevity of the hollow structure by preventing it from drying out in ambient conditions. We further explored the pneumatic morphing capabilities of these hollow structures, demonstrating their ability to change shape when inflated, and investigated their potential as functional sensors, including stretch, displacement, and touch sensors.

Our main contributions are:

- We propose a novel, low-cost, DIY-friendly, and accessible fabrication pipeline for making tubular hollow alginate structures with customizable shapes, cross-sectional geometry, and stiffness using progressive crosslinking.
- We establish a set of functional primitives for hollow tubular alginate, including shape, morphing, and sensing.
- We demonstrate the versatility and design possibilities of BioTube through five application examples, showcasing its potential in shape-changing interfaces, culinary design, transient wearables, etc.

2 Related Work

2.1 Biodegradable Materials in HCI

The HCI community is increasingly prioritizing sustainability to reduce the environmental impact of design processes. Researchers advocate for repurposing waste materials to minimize raw material use [23, 101] and exploring "unmaking" practices, that focus on material reuse [6, 87, 108]. Additionally, the development of biodegradable materials like mycelium [30, 99, 100, 105], kombucha [4, 68], play-dough [9], food-waste bioclays [5], gelatin [43, 46, 47], agar [3], coffee grounds [79], and alginate [43, 70, 121], offers promising solutions for reducing waste in sustainable HCI. These materials have been utilized in I/O interfaces [3, 5, 30], wearables [4, 68, 100, 121], shape-changing interfaces [58, 60, 70], actuators [17, 78, 92, 107], sensors [12], heating interfaces [86], energy storage devices [59, 88], enclosures [99], etc.

Various fabrication techniques, including 3D printing [9, 79, 92], fiber spinning [46, 121], casting and molding [43, 47, 70, 99], have been explored to manipulate these biodegradable materials. Given the underlying DIY culture of using biodegradable materials, simple material preparation processes without the need for lab-grade chemicals and dangerous manipulations [70] as well as accessible manual or hands-on fabrication techniques [5, 47] are greatly appreciated in the maker community.

In our work, we investigate alginate as a material candidate, focusing on its crosslinking features for making biodegradable devices, and contribute to the ongoing exploration of accessible fabrication techniques for biodegradable materials in HCI.

2.2 Design with Hollow Structures

Devices with hollow structures are gaining significant interest in the HCI community, particularly for applications like inflatable chambers that enable actuators or shape-changing interfaces. Various materials and fabrication methods have been explored, including thermoplastic (fabric) films with heat-sealing [14, 57, 71, 82, 110, 113], PLA via FDM printing [104], flexible resin with SLA printing [111], paper-silicone composite with casting [63, 114], alginate with embedded 3D printing [92] or molding and casting processes [70].

Hollow structures can also serve various sensing functions, such as pressure and strain sensing with liquid metal embedded in elastomer-cast microchannels [74, 91]; acoustic sensing through airflow-induced sounds in designed cavities [34, 94]; and pneumatic [95] or capacitive sensing [83] in 3D printed objects.

Hollow structures can also contain diverse fluids for interactive purposes: liquid metal in silicone channels for interactive electrical components [96], flavored liquids in molded agar jelly for enhanced food interactions [20], and thermofluidic channels for thermochromic displays [116]. Beyond the field of HCI, hollow structures are commonly used as microfluidic channels, fabricated by creating and subsequently removing sacrificial channels within a PDMS substrate [32, 35].

Notably, *hollow tubular structures* show promise in applications such as pneumatic actuators [38], McKibben muscles [42], biotextiles [22], and dynamic fluid-based displays [54].

In terms of fabrication techniques, the industry has well-established methods for extruding polymeric materials into tubes [39], and the maker community has explored DIY approaches for creating

silicone tubes [98]. However, these techniques primarily aim to produce durable tubes for long-term use, and there remains a lack of DIY-friendly methods for fabricating hollow tubular structures with biodegradable materials. In this paper, we contribute by introducing a novel fabrication pipeline for creating functional hollow tubular devices with biodegradable alginate hydrogel and exploring their transient and sustainable design potential within the HCI context.

2.3 Fabricating Hollow Tubular Alginate

Various forms of alginate, such as films [43, 70], pastes [43], fibers [121], and molded parts [70], have been explored in the HCI community. However, hollow tubular alginate remains relatively understudied.

Beyond HCI, several methods have been developed to fabricate hollow tubular alginate. The coaxial device-based method provides a straightforward approach, where two fluid streams—typically alginate in the sheath and a core fluid like calcium solution [13, 51, 109, 117] or inert materials such as aqueous starch [64], mineral oil [69], or PVA [122]—flowing concentrically to form a solid alginate shell around a fluid core. This method is adaptable for use in microfluidic spinning to harvest continuous hollow fibers [26, 36, 48, 65, 76] and 3D printing to create hollow fiber scaffolds [28, 52, 61] and vessel-like structures [29]. However, maintaining coaxial alignment and the complexity of the setup pose challenges.

Alternative methods include template-based approaches. For example, cyclically dipping a metal rod into alginate and calcium solutions can create alginate tubes [31]. However, successfully removing such non-sacrificial templates restricts the geometry of hollow structures. Alternatively, placing sacrificial templates (e.g. gelatin) containing calcium cations into alginate can form a shell on the crosslinking interface [72, 90, 106], after which the template can be removed by melting. Nevertheless, fabricating complex template (e.g. helical) geometries can still be challenging. Moreover, the calcium solution can serve as a "dynamic template" when extruding into the alginate and controlling its growing direction [103]. However, this method's geometry control is complicated because it requires rotation of the alginate solution. Another method involves using microfiltration membranes as templates that induce radial crosslinking [115], yet it demands complex equipment.

In summary, our method offers a straightforward, accessible, and customizable approach for fabricating hollow tubular alginate, expanding its potential applications in HCI.

3 Design Space

We synthesized the design space of BioTube in Figure 2.

Workflow. The BioTube workflow is based on a progressive crosslinking process: when exposed to calcium ions, the alginate fiber gradually crosslinks from the outside in. After a brief initial crosslinking period, the alginate fiber remains hollow with an uncrosslinked core that can be removed. The fiber diameter can be adjusted by using different needle gauges for extrusion, while the shell thickness is controlled by varying the initial crosslinking duration. Further crosslinking allows for customization of the fiber's shape, cross-sectional profile, and stiffness. Additionally, a solvent exchange method can be employed to extend the alginate lifespan. The workflow's detailed steps are outlined in Section 4.

Functional Primitives. We categorized the hollow tubular alginate's functional possibilities into three primitives:

- **Shape Primitives**: Alginate tubes can be shaped using the *reshaping crosslinking* process for 2D patterns and 3D geometries like helices or with thread-based techniques such as braiding, weaving, and knitting (Section 6.1).
- **Morphing Primitives**: By applying *reshaping and asymmetric crosslinking* techniques, we can enable the alginate to change shape when inflated with air or liquid (Section 6.2).
- **Sensing Primitives**: Alginate tubes can also be used as transient sensors, including optical press displacement, resistive stretch, and capacitive touch sensors (Section 6.3). The hollow structure of the alginate enables optical displacement sensing by utilizing the internal cavity to transmit light and detect changes in light intensity. For resistive stretch sensing, the tubular alginate fiber demonstrates improved sensitivity compared to solid alginate fibers.

Applications. By applying different crosslinking strategies and functional primitives, we explored various transient applications using the proposed workflow (Fig. 18). For example, we applied optical displacement sensing for eco-friendly interactive glowing bracelets, stretch sensing to enhance glove interactivity, and morphing capabilities for shape-changing confections and grippers.

4 Fabricating BioTube

BioTube utilizes the external gelation technique, also known as the "direct spherification" in modernist cuisine or the "diffusion method". In this process, alginate is dripped or extruded into a calcium bath, where calcium ions gradually diffuse into the alginate, creating a crosslinking zone that progresses from the surface inward [11, 55, 77]. Building on this principle, we developed a progressive crosslinking method (Fig. 3).

4.1 Material Preparation

We provided step-by-step illustrations for the material preparation in Figure 3 (a). Following a method similar to that described in [121], we prepared a 4 wt.% (weight percent) sodium alginate solution by mixing 2g sodium alginate powder (SKU:1061-50, Modernist Pantry), 48g tap water, and two drops of food dye (AmeriColor) in an AS ONE Disposable Cup (Vacuum Type, 100mL) using a lab overhead stirrer (JJ1 precise strength power mixer, approximately 400 RPM) for one hour. The solution was transferred into a 60-mL syringe (Easy Glide) and placed upright for at least 3 hours (or refrigerated overnight) to allow air bubbles to rise. Before use, the plunger was pushed to expel the top bubbles. The prepared alginate can be refrigerated and stored for up to one week. If refrigerated, the syringe should be left at room temperature for one hour (20±4°C, as the alginate temperature might affect the crosslinking speed characterized in Figure 4). Finally, a stainless steel luer lock needle was attached to the syringe (a 10-gauge needle was used throughout this paper unless otherwise specified).

4.2 Initial Crosslinking

First, we prepared 800 grams of 1 wt.% calcium chloride ($CaCl_2$) solution (ALDON Innovating Science) in a Crystallizing Dish (PYREX No.3140, 150mm diameter, 75 mm height). The alginate was then

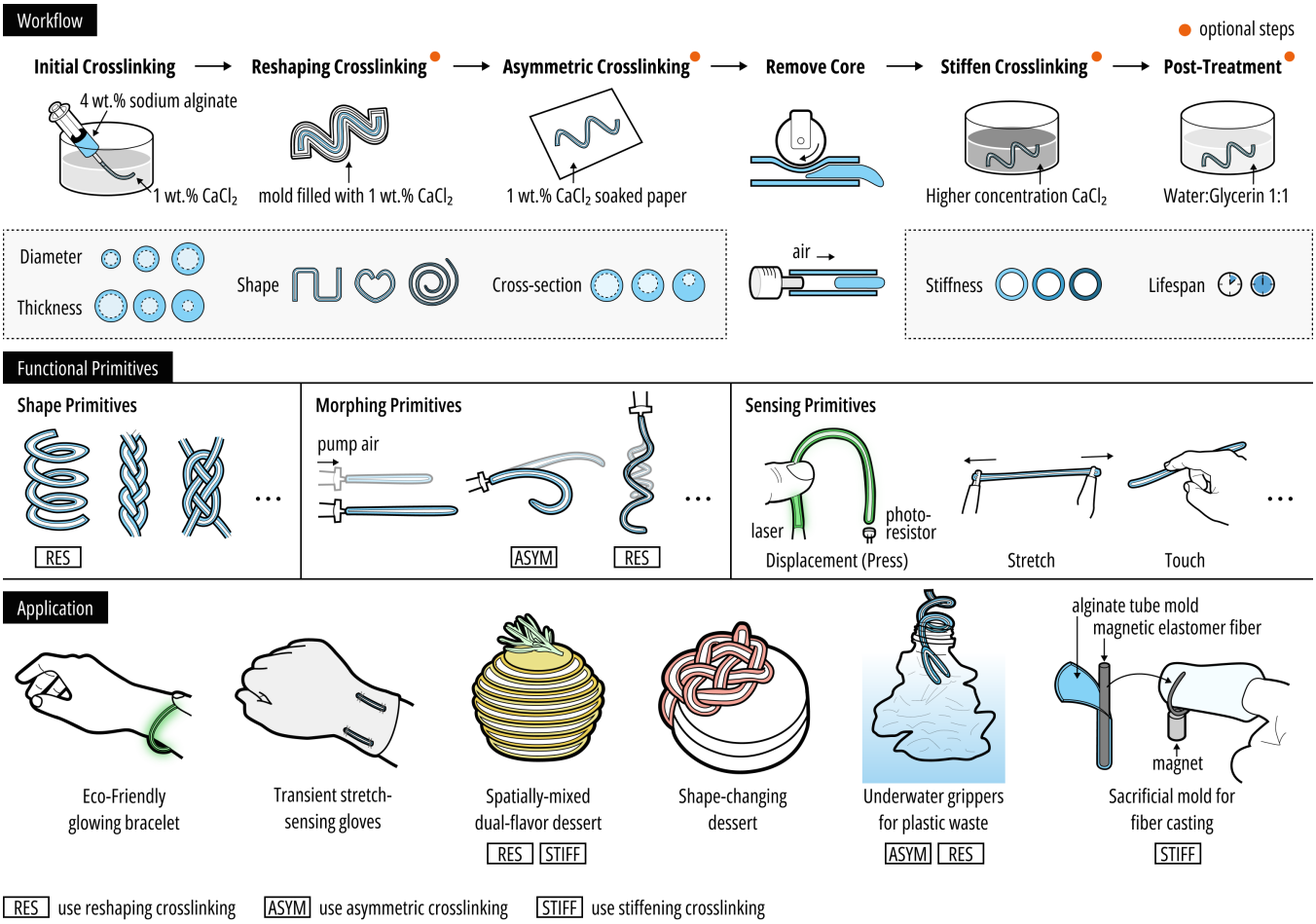

Figure 2: BioTube design space.

extruded into the calcium solution either manually or using a syringe pump. By adjusting the crosslinking time of the alginate fiber in the calcium solution, we can produce alginate tubes with varying shell thicknesses, as characterized in Figure 4. The fibers can be cut to any desired length, as the calcium solution quickly seals the ends by crosslinking the exposed alginate. After crosslinking, the alginate fibers were removed from the calcium solution and rinsed thoroughly with tap water for 10 seconds to remove excess calcium ions.

4.2.1 pump extrusion. We designed a syringe pump setup suitable for extruding high-viscosity alginate materials (Fig. 3 b, pump extrusion) based on an open-source syringe pump design [16]. In the previous work, horizontal setups were used for wet-spinning lower-concentration alginate solutions [121]. However, these setups were unsuitable for extruding higher-concentration alginate because the highly viscous solution had to pass through additional silicone tubing and connectors, causing increased friction and making extrusion difficult. To address this, we adopted a vertical syringe configuration, allowing the dispensing needle to be inserted directly into the solution, minimizing friction and enabling smoother extrusion. We used a Nema 17 bipolar stepper motor controlled by an Arduino Uno and an Adafruit TB6612 motor driver board. The motor speed was set to 1.37 RPM to achieve a flow rate of 6 mL/min for the alginate. Detailed information on the machine design and hardware setup is available in the GitHub documentation[1].

Using our Arduino code[2], users can control the stepper motor to either continuously extrude alginate fibers or specify a desired fiber length. For a specified tube length (l_{tube}), the number of steps ($n_{extrusion}$) required for the stepper motor can be calculated as follows:

$$n_{extrusion} = l_{tube} \cdot \frac{r_{needle}^2}{r_{syringe}^2} \cdot \frac{N_{steps}}{p} \cdot e$$

where r_{needle} is the inner radius of the needle, $r_{syringe}$ is the inner radius of the syringe, p is the pitch of the lead screw, N_{steps} is the total number of discrete steps the stepper motor completes in one full revolution, and e is the extrusion multiplier accounting for the

[1]https://github.com/biotube-alginate/pump
[2]https://github.com/biotube-alginate/pump/tree/main/code

Figure 3: BioTube fabrication workflow.

die swell effect during alginate extrusion (based on our experiments, $e \approx 1.325$ when using a 10-gauge needle).

Similar to the wet spinning setup described in [121], a magnetic stir bar (CHSZCHC 9×35mm) was placed inside the calcium bath, which was positioned on a stirring plate (GLASSCO Magnetic Stirrer 900DGCR01, set to 150 RPM) to provide initial drawing for fiber formation.

4.2.2 manual extrusion. To enable users to quickly prototype or test our method without a complex machine setup, we explored a manual extrusion method as an alternative to the pump extrusion (Fig. 3 b, manual extrusion). In this approach, the syringe was held steady using the index and middle fingers on the syringe tab while the thumb applied even pressure to push the plunger. The syringe was positioned at a fixed angle of approximately 45 degrees relative to the horizontal plane, with the dispensing needle submerged in the calcium solution. Through our experiments, we observed that tilting the syringe during extrusion helped prevent alginate clogging in the needle, even without a magnetic stirrer. This is likely because the tilt angle imparted an initial drawing velocity to the fiber, similar to the effect of the magnetic stirrer. To ensure steady extrusion, the syringe was pushed at a consistent rate of approximately 0.1 mL/s, estimated by observing the plunger displacement of 1 mL over 10 seconds. We evaluated and compared the manual extrusion method with the pump extrusion setup (Fig. 5), demonstrating their similar consistency in tube formation.

4.3 Further Crosslinking, Core Removal, and Post-Treatment

4.3.1 Reshaping Crosslinking. The fibers can be reshaped using a mold and further crosslinked, allowing the newly crosslinked alginate to conform to and "memorize" the new shape (Fig. 3 c, reshaping crosslinking). Alginate fibers were initially crosslinked for 10 seconds before being transferred to a mold filled with a 1 wt.% $CaCl_2$ solution for further crosslinking. For 2D shapes, we developed a design tool to generate molds for reshaping crosslinking from planar paths, which will be detailed in Section 6.1. As characterized in Section 5.2.1, desirable shape retention could be achieved after 1 minute of further crosslinking.

4.3.2 asymmetric crosslinking. We could locally adjust the shell thickness using asymmetric crosslinking (Fig. 3 c, asymmetric crosslinking). Alginate fibers were initially crosslinked for 10 seconds, thoroughly rinsed with tap water for another 10 seconds, then transferred to or wrapped with a piece of weighing paper (VWR) that had been pre-soaked in a 1 wt.% $CaCl_2$ solution for 5 seconds. The alginate fiber can be placed directly on a piece of calcium-soaked paper to thicken the bottom part or wrapped with calcium-soaked paper to increase the shell thickness in specific sections, as characterized in Section 5.2.2. The maximum length of the alginate fiber that can be asymmetrically crosslinked is constrained by the size of the weighing paper. However, multiple pieces of calcium-soaked paper could be placed side by side to accommodate longer fibers, as demonstrated in Figure 14 (b1). The paper served as a stable diffusion interface for calcium cations, enabling localized crosslinking. Weighing paper was selected for its durability when wet.

4.3.3 core removal. The uncrosslinked alginate core could be removed either by pushing with a roller or by pumping air into one end using a syringe (Fig. 3 d).

In the roller method (Fig. 3 d, roller), the fiber was cut open at one end with a craft knife. A custom-designed 3D-printed roller[3] was then used to push out the uncrosslinked core. For longer fibers, the removal process was performed incrementally to prevent excessive accumulation of alginate, which could cause the tube to rupture.

[3]https://github.com/biotube-alginate/pump/tree/main/model/roller

The process started by pushing out about 10 cm of the core closest to the opening, then progressively increased to 20 cm, 30 cm, and so on. The longest fiber (initially crosslinked for 3 minutes) from which we successfully removed the core using the roller method was approximately 148 cm (Fig. 25 b).

In the syringe method (Fig. 3 d, syringe), both ends of the alginate fiber were cut open using a craft knife. A syringe with a suitably sized needle (chosen based on the tube's inner diameter — small enough to fit but large enough to minimize leakage) was inserted into one end. Users could pinch the connection point to reduce leakage if needed. The syringe was then pushed gradually at a rate of approximately 0.1 mL/s, forcing the uncrosslinked alginate out through the opposite end. This method is suitable for shorter fibers or fibers with complex geometries where using the roller would be challenging (Fig. 21 a2). However, unlike the roller method, it does not allow for incremental core removal, which may cause material accumulation when working with longer fibers, potentially leading to tube rupture. The longest fiber (initially crosslinked for 3 minutes) from which we successfully removed the core using the syringe method was approximately 39 cm; attempts with longer fibers resulted in rupture.

4.3.4 stiffening crosslinking. After core removal, the alginate tube can be further crosslinked in an 8 wt.% calcium solution for 10 minutes to enhance its stiffness (Fig. 3 e), as characterized in Section 5.2.3. This stiffening effect occurs because higher calcium concentrations increase the stiffness of alginate until saturation is reached [10, 40, 50].

4.3.5 post-treatment. Like other hydrogels, alginate tends to dry out under ambient conditions. To prevent this, we employed a solvent displacement method similar to that described in [85] to extend the shelf life of hollow alginate tubes. Specifically, the alginate was immersed in a glycerin-water mixture at a 1:1 volume ratio for 20 hours (Fig. 3 f). As detailed in Section 5.3, this method effectively prevented the alginate tubes from drying out for at least 14 days.

5 Mechanism

In this section, we present a detailed characterization of the mechanisms involved the fabrication workflow. For all quantifiable evaluations in subsequent sections, we used the pump extrusion method with parameters specified in Section 4.2.1.

5.1 Initial Crosslinking

To evaluate the shell formation during the initial crosslinking, we prepared sodium alginate at different concentrations (0.5 wt.%, 2 wt.%, 4 wt.%) using local tap water. The 0.5 wt.% concentration is typical for basic spherification [7], while 2 wt.% [121] and 4 wt.% [97] concentrations are used in wet spinning to enhance alginate mechanical properties. We used 1 wt.% $CaCl_2$ bath, which is commonly used in food preparation [7, 49]. This relatively low calcium concentration slows the crosslinking process [10], allowing for finer control over shell thickness.

The alginate was extruded into the calcium bath at room temperature (20±4°C for both the alginate and calcium solution) using the syringe pump with a 10-gauge needle at a flow rate of 6 mL/min. The syringe pump operated for 1 second, producing an alginate fiber approximately 15 mm long, which was crosslinked for varying durations. Then, the fiber was rinsed with tap water for 10 seconds, and the uncrosslinked core was removed using the roller method. Five 1mm-thick samples were evenly sliced along the fiber's length from the beginning to the end. The shell thicknesses of these samples were measured using a digital microscope (TOMLOV 1200X) (Fig. 4 a). The initial crosslinking produced an alginate shell with uniform thickness and a circular shape, with the shell thickness increasing over the crosslinking time (Fig. 4 b). All alginate concentrations formed an immediate shell (within 10 seconds) upon contact with calcium ions, consistent with previous studies [49]. Wall thickness increased linearly with crosslinking time across all concentrations (R^2 = 0.98, 0.98, 0.99 for 0.5 wt.%, 2 wt.%, and 4 wt.%, respectively). Higher alginate concentrations slowed the crosslinking process, likely due to the denser network hindering calcium ion diffusion [10].

We also tested various needle gauges to extrude 2 wt.% alginate, taking advantage of its low viscosity and easier extrusion with larger gauge needles, while 4 wt.% alginate proved too viscous to extrude with needles larger than 14 gauge. The smallest hollow fiber obtained was extruded using a 20-gauge needle (0.603 mm inner diameter) and crosslinked for 1 second (Fig. 4).

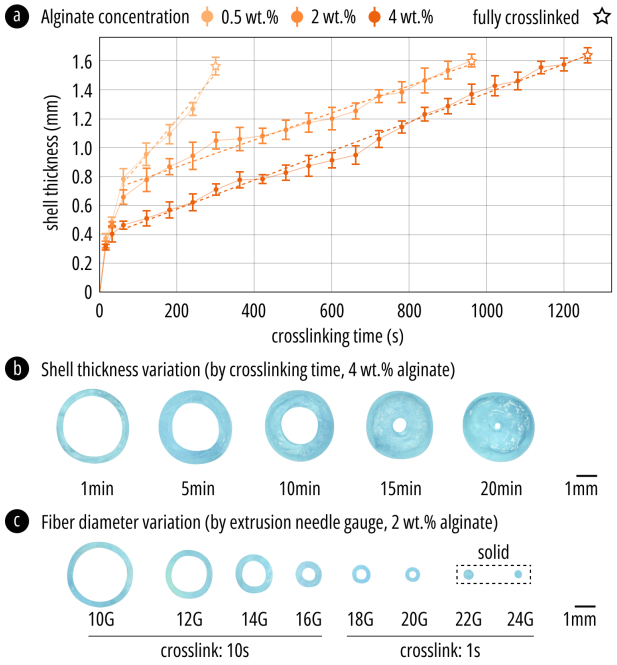

Figure 4: Initial crosslinking evaluation in 1 wt.% $CaCl_2$ solution. (a) Shell thickness growth of alginate fibers extruded with a 10-gauge needle under varying crosslinking times and alginate concentrations. (b) Cross-sections of 4 wt.% alginate hollow fibers at various crosslinking times. (c) Cross-sections of 2 wt.% alginate hollow fibers extruded with different needle gauges, with the smallest hollow fiber obtained using a 20-gauge needle.

Using the pump and manual extrusion methods described in Section 4.2, we extruded five 150mm-long 4 wt.% alginate fibers using the 10-gauge needle and let them crosslinked for 5 minutes. Each fiber was evenly sampled along its length and sliced into four 1mm-thick sections to measure the outer diameter and shell thickness (Fig. 5). While prior work [121] highlighted challenges in achieving consistent alginate fiber extrusion using hand-held syringes, we found that the manual method produced tubes with comparable uniformity in diameter and shell thickness to those extruded using the pump. However, the fibers produced manually had a slightly larger outer diameter, likely due to the absence of the pulling force generated by the magnetic stirrer. We hypothesize that this consistency arose from the higher viscosity of the alginate solution used in our experiments. The increased viscosity requires greater force for extrusion, which slows down the process and allows for better control over the extrusion speed. This inherent resistance helps to stabilize the manual extrusion rate, making it easier to achieve consistent results even without mechanical assistance.

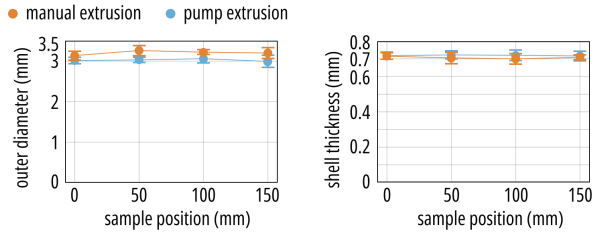

Figure 5: Comparison between the pump and manual extrusion of 4 wt.% alginate into 1 wt.% $CaCl_2$ solution with a 10-gauge needle. Extrusion method detailed in Section 4.2.

Additionally, we conducted basic mechanical tests for sodium alginate used in our study. First, we evaluated the viscosity of the sodium alginate at different concentrations with a digital rotary viscometer (Saladulce NDJ-9S) (Fig. 6 a). All concentrations were tested at 22°C. The rotor type and speed for each alginate concentration group were selected based on the viscometer's user manual to ensure accurate measurements: 0.5 wt.% alginate (rotor 1, 30 RPM), 1 wt.% alginate (rotor 1, 6 RPM), 2 wt.% alginate (rotor 2, 3 RPM), 3% alginate (rotor 3, 3 RPM), and 4 wt.% alginate (rotor 3, 0.6 RPM). Here, we measured the alginate solution's apparent viscosity (fluid viscosity at a specific shear rate and temperature). Previous studies have demonstrated a power-law relationship between specific viscosity (η_{sp}) and concentration of alginate solutions, expressed as $\eta_{sp} \sim C^n$. The specific viscosity is given by $\eta_{sp} = \frac{\eta_0 - \eta_s}{\eta_s}$, where η_0 is the zero-shear viscosity (the viscosity at near-zero shear rate) and η_s is the solvent viscosity [25, 62]. Alginate solutions also exhibited non-Newtonian, shear-thinning behavior, where the viscosity decreases with increasing shear rate [25, 81]. This property benefited our extrusion-based fabrication process by enabling smoother nozzle flow. As demonstrated in Section 4.2, both the custom-built syringe pump and even manual operation proved effective in extruding 4 wt.% alginate.

Moreover, we evaluated the tensile properties of three groups of hollow tubular alginate fibers, prepared with 4 wt.% alginate and different initial crosslinking times, using a digital force push-pull gauge (Mxmoonfree HJJ-001) at a stretching speed of approximately 0.5 mm/s (Fig. 6 b). After the initial crosslinking, all alginate fibers were further crosslinked in a 1 wt.% $CaCl_2$ solution for 10 minutes to reach diffusion equilibrium [102]. Each alginate fiber measured 50 mm in total length, with 10 mm clamped at each end, leaving a 30 mm central section for stretching. For each group, 5 samples were tested. We excluded data below 40% strain from our analysis, as the measured force in this range was below the minimum measurable force of the push-pull gauge used in our experiment. Across all groups, the alginate tubes exhibited a similar Young's modulus of approximately 0.83 MPa. However, alginate fibers with a 5-minute initial crosslinking stretched up to 140% strain, whereas those with 10-minute and 20-minute initial crosslinking broke at around 110% strain.

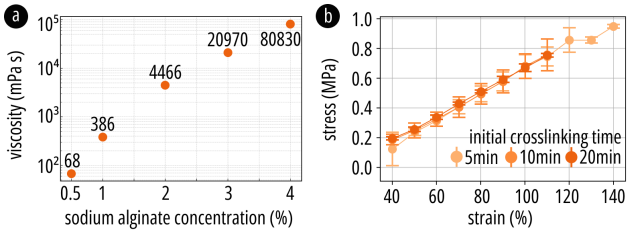

Figure 6: Basic mechanical tests. (a) Viscosity of sodium alginate at different concentrations. (b) Stress-strain curves of 4 wt.% alginate hollow fibers with varying initial crosslinking times.

Unless otherwise specified, we will use 4 wt.% alginate for the remainder of this paper due to its ease of relatively precise wall thickness control and the enhanced robustness of the resulting gel, which prevents breakage during core alginate removal.

5.2 Further Crosslinking

5.2.1 reshaping crosslinking. We set the initial crosslinking time to 10 seconds, then transferred the alginate fiber into a 3D-printed mold filled with 1 wt.% $CaCl_2$ solution for further crosslinking. Two reshaping primitives were evaluated: a "sharp bend" (90-degree angle) and a "continuous curvature" (180-degree bend with a radius of 30mm), with five samples tested for each. After various crosslinking times, the alginate was removed from the mold and floated on a 10 wt.% glucose solution to eliminate external forces and reveal its retained shape (Fig. 7 a, b). Shape retention was then calculated using the formula: $\textit{shape retention rate} = \frac{\Delta\theta}{\theta_0}$, where $\Delta\theta$ was the actual angle change and θ_0 is the desired angle change (90° for the sharp bend and 180° for the continuous curvature). We found that both primitives exhibited desirable shape retention after 1 minute of further crosslinking, with the alginate achieving continuous curvature more quickly. Although we did not measure the change in shell thickness of the hollow tubular alginate during the reshaping crosslinking process, it is expected to be similar to the results shown in Figure 4, as both processes involve crosslinking alginate fibers in a solution-based environment.

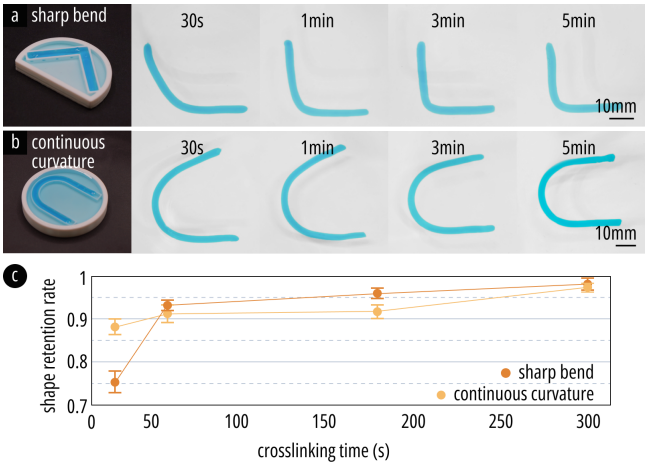

Figure 7: Reshaping crosslinking evaluation. Alginate fibers were initially crosslinked for 10 seconds and then placed in a mold filled with 1 wt.% $CaCl_2$ for further crosslinking. (a) Sharp bend reshaping. (b) Continuous curvature reshaping. (c) Shape retention rate over the further crosslinking time.

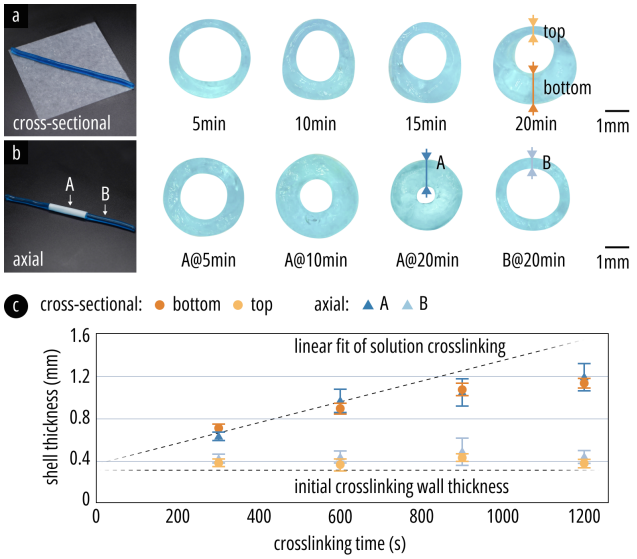

Figure 8: Asymmetric crosslinking evaluation. 1 wt.% $CaCl_2$-soaked weighing paper was placed in contact with alginate fibers (initially crosslinked for 10 seconds) to induce localized further crosslinking. (a) Cross-sectional asymmetry. (b) Axial asymmetry. (c) Shell thickness changes in areas in contact with the paper versus areas not in contact for both groups, over the further crosslinking time.

5.2.2 asymmetric crosslinking. We evaluated two primitives for asymmetric crosslinking: cross-sectional and axial asymmetry (Fig. 8). As described in Section 4.3.2, weighing paper was dipped into 1 wt.% $CaCl_2$ solution for 5 seconds before use. We prepared 5cm-long alginate fibers initially crosslinked for 10 seconds, followed by a 10-second rinse with tap water for testing. In the cross-sectional group, the prepared weighing paper was placed beneath the alginate fiber. After further crosslinking for varying durations, the core was removed using the roller method. Five evenly spaced 1mm-thick samples were sliced along the fiber from the beginning to the end. In the axial group, five alginate fibers were prepared by wrapping a 1.5-cm-wide paper around the center of each fiber three times. After further crosslinking and core removal, each of the five alginate fibers was sampled by slicing a 1mm-thick section from the center of the wrapped area and another from the non-wrapped area, 2 mm away from the wrapped area.

The weighing paper successfully induced localized crosslinking: the side in contact with the calcium-soaked paper became thicker (Fig. 8 a), and in the axial group, the wrapped section also showed increased wall thickness (Fig. 8 b). This asymmetric crosslinking allowed for localized tuning of shell thickness, with areas not touching the calcium-soaked paper maintaining stable thickness (Fig. 8 c). However, the rate of thickness increase slowed compared to crosslinking in solution (refer to the linear fit line in Fig. 8 c, which is based on data from Fig. 4), likely due to the gradual depletion of calcium ions from the paper.

5.2.3 stiffening crosslinking. To evaluate stiffening crosslinking, alginate samples underwent an initial 10-minute crosslinking, followed by core removal using the roller method, and then a 10-minute further crosslinking in varying $CaCl_2$ concentrations (1 wt.%, 2 wt.%, 4 wt.%, 8 wt.%). A custom linear movement pusher was then used to cyclically compress and release 40-mm-long hollow tubular alginate samples, with diameter deformation set to 8%. The strain gauge on a Precision Electronic Balance (U.S.SOLID) measured the applied force over 10 push-release cycles to record peak compression force (Fig. 9). Five alginate samples for each calcium concentration treatment were tested. The results showed that higher calcium concentrations increased the stiffness of the alginate, requiring more force to achieve the same deformation.

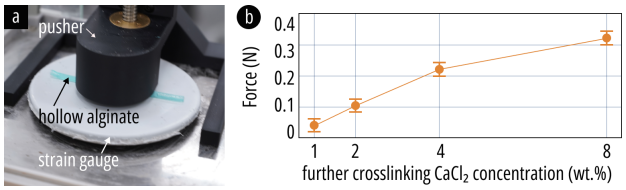

Figure 9: Stiffening crosslinking evaluation. Alginate fibers were initially crosslinked for 10 minutes, the core was removed, and they were further crosslinked in varying concentrations of $CaCl_2$ solution for another 10 minutes. (a) Setup for stiffness evaluation using a precision electronic balance. (b) Force required to achieve the same 8% diameter deformation in alginate fibers treated with different $CaCl_2$ concentrations.

5.3 Post-Treatment

To evaluate the post-treatment effect, we prepared hollow alginate fibers by immersing them in a glycerin-water mixture at a 1:1 volume ratio for 20 hours after an initial 10-minute crosslinking, allowing glycerin to partially replace the water. Five 3-cm-long alginate samples were prepared for both the glycerin-treated and untreated groups, and their weight changes were monitored over time. Additionally, five cross-sectional samples (same as the sampling method from Section 5.1) from the glycerin-treated group were analyzed for wall thickness over time.

This process effectively prevented the alginate from drying out when left in an open ambient environment (Fig. 10 a, the alginate returned to the transparent state as the dye leached out during the solvent exchange), helping it retain its weight and hollow structure (Fig. 10 c). In contrast, alginate without this treatment dried out in 8 hours to a thin sheet and lost the hollow structure (Fig. 10 b).

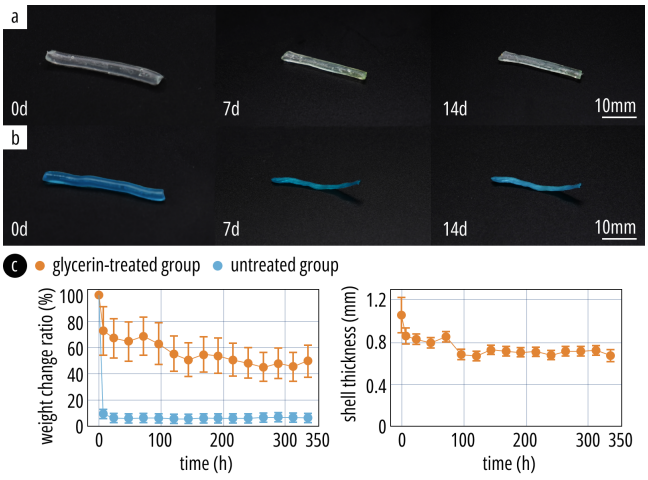

Figure 10: Post-treatment evaluation. Alginate fibers were initially crosslinked for 10 minutes and split into two groups—one untreated and one immersed in a 1:1 glycerin-water mixture for 20 hours. Images of the glycerin-treated (a) and untreated (b) alginate on day 0, day 7, and day 14 in an open environment. Weight change over time for both groups (c, left), and shell thickness of the treated alginate over time (c, right). The shell thickness of untreated fibers was not measured, as they dried out and lost their hollow structure within 8 hours.

6 Functional Primitives

6.1 Shape Primitives

The hollow tubular alginate can be formed into various shapes.

First, through the reshaping crosslinking process (Section 5.2.1), both 2D and 3D geometries can be created using molds (Fig. 11 a). To simplify the mold-assisted 2D shaping process, we developed a mold design tool using Rhinoceros 3D and Grasshopper, which allows users to convert 2D paths into customized molds for reshaping crosslinking (Fig. 12). Users begin by inputting their desired 2D

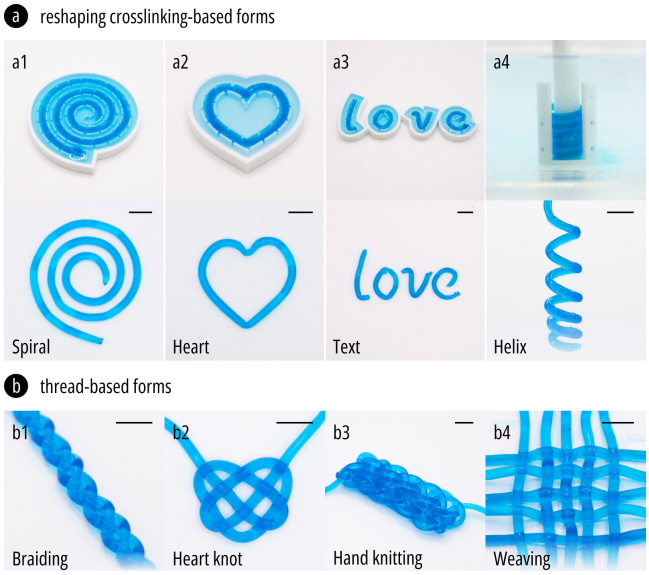

Figure 11: Shape primitives of BioTube. (a) Through the reshaping crosslinking process, both 2D (a1-a3) and 3D (a4) geometries can be created using customized molds. (b) The hollow tubular alginate can be shaped like regular threads to achieve more complex forms such as braiding (b1), tying knots (b2), knitting (b3) or weaving (b4). (Scale bar: 10mm)

paths and alginate fiber radius (Fig. 12 a). After selecting the target geometry, the tool generates retaining walls to hold the tube's shape and contain the $CaCl_2$ solution (Fig. 12 b). Gaps are then introduced in the inner wall to allow the $CaCl_2$ solution to replenish calcium ions (Fig. 12 c, e3). Finally, a 3D mold is generated, which can be printed using a 3D printer (Fig. 12 d). The alginate fibers shown in Figure 11 (a) were initially crosslinked for 10 seconds and then placed in the mold for an additional 10 minutes of reshaping crosslinking.

Second, the hollow tubular alginate can also be shaped like a regular thread (Fig. 11 b). In this case, all alginate fibers underwent only a 30-second initial crosslinking. More complex forms can be achieved by braiding, tying knots, knitting, or weaving the alginate fiber, allowing for intricate and flexible designs.

6.2 Morphing Primitives

The hollow tubular alginate exhibits distinct shape-changing capabilities when inflated. We used a 1/16" luer hose barb adapter (BleedZone) to connect the hollow alginate to the syringe (Fig. 13 b). The shell thickness at the connection point must be sufficiently large to ensure a secure attachment that remains intact during actuation. Based on our observations, for alginate extruded with a 10-gauge needle, a minimum of 5-minute uniform crosslinking around the connection area provided adequate thickness. However, in cases where alginate fibers were asymmetrically crosslinked with calcium solution-soaked paper (e.g., Fig. 14 a2), this uniform thickness is not achieved at the connection point. To address this, we applied the axial crosslinking method from Figure 8 (b) (by

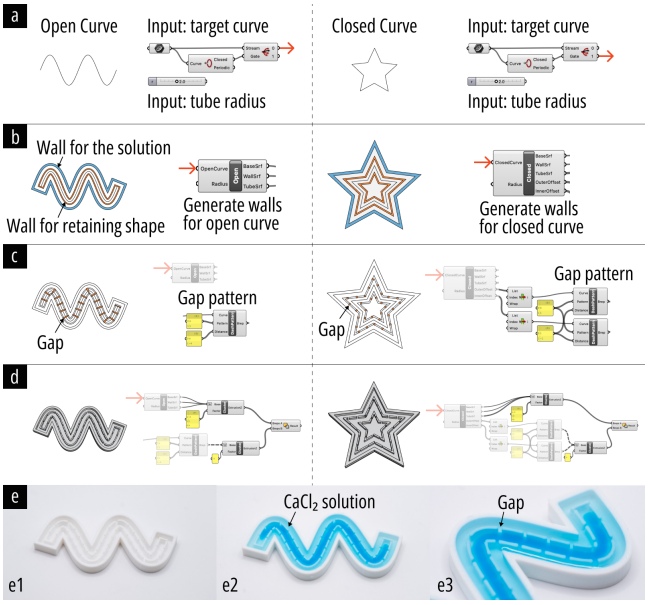

Figure 12: Mold design tool for shaping alginate fibers into 2D geometries via reshaping crosslinking. (a) Users input 2D curves and set the alginate radius. (b) Walls are generated to retain the alginate shape and contain the $CaCl_2$ solution. (c) Gaps in the walls are created to allow the $CaCl_2$ solution to replenish calcium ions inside the inner walls, ensuring consistent crosslinking of the alginate fibers. (d) The final mold is generated and can be exported for 3D printing. (e) Printed mold and an example of usage.

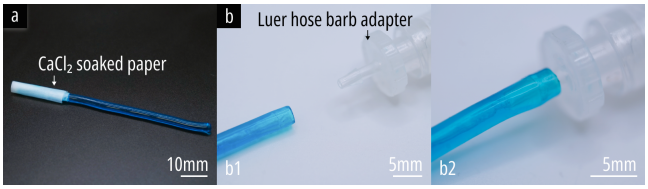

Figure 13: Connection of the air source (a syringe, in our case) to the hollow tubular alginate. (a) Calcium-soaked paper wrapped around the end of the alginate fiber to locally thicken the wall, ensuring a more secure connection to the adapter. (b) The alginate fiber is connected to the syringe using a luer hose barb adapter.

wrapping calcium-soaked paper around the fiber three times) to locally increase the shell thickness (Fig. 13 a), ensuring a secure connection.

The morphing capabilities are categorized into three basic primitives: extension, bending, and unbending (Fig. 14 a). For each crosslinking time in these three primitive categories, five samples were tested.

- **Extension**: Alginate subjected only to initial crosslinking elongates when inflated with air. This elongation decreases as the wall thickness increases with longer crosslinking times (Fig. 14 a1). For alginate fibers with a 30-second initial crosslinking, the fiber was rinsed with tap water for 10 seconds and then wrapped with calcium-soaked paper to further crosslink the adapter connection area for 4 minutes and 30 seconds (in total 5 minutes).
- **Bending**: Achieved through cross-sectional asymmetric crosslinking (Fig. 8 a), where the tube expands more on the side with the thinner wall. As further crosslinking time increases, so does the wall thickness difference, resulting in greater bending. However, this also reduces the hollow volume, making the alginate more prone to rupture (Fig. 14 a2). For instance, samples with 900-second further crosslinking ruptured between 0.6-0.7 mL of air at atmospheric pressure, while those with 600-second crosslinking ruptured between 0.9-1 mL of air at atmospheric pressure.
- **Unbending**: Reshaped alginate straightens when air is pumped into it (Fig. 14 a3). As the further crosslinking time increases, the hollow chamber shrinks, making the unbending effect more pronounced under the same air volume at atmospheric pressure. For alginate fibers with a 60-second initial crosslinking, the fiber was rinsed with tap water for 10 seconds and then wrapped with calcium-soaked paper to further crosslink the adapter connection area for 4 minutes (total crosslinking time of 5 minutes).

Built on these basic primitives, we can build various more complex pneumatic shape-changing primitives with different further crosslinking strategies (Fig. 14 b).

All the samples in the Figure 14 were prepared using a 10-gauge needle and a 30-second initial crosslinking under room temperature, inflated by air. The basic primitives in Figure 14 (a) were evaluated using 5 cm long tubular alginate (excluding the connection part) within 30 minutes after preparation, with each curve in the graphs representing averaged data from three independent samples with varying crosslinking times. Lastly, all samples in Figure 14 (b) underwent a 5-minute further crosslinking.

These morphing primitives could be repeatedly inflated and deflated to achieve shape changes. To demonstrate this, we evaluated the repeatability of the shape change, using the bending primitive as an example (Fig. 15). The sample, taken from the 300-second further crosslinking group in Figure 14 (a2), was subjected to cyclic air inflation of 0.5 mL (at an average rate of 0.5 mL/s) within 30 minutes after preparation, with the resulting bending angle recorded. Over 200 cycles, the bending angle remained consistent, with only a slight decrease observed in the final 25 cycles. The sample eventually ruptured after 200 cycles. Notably, the sample exhibited a larger bending angle than the data in Figure 14 (a2) (which reflects the bending angle measured during the first-time inflation), likely due to the plastic deformation after the full-range inflation to 1 mL. Nonetheless, the sample continued to demonstrate good repeatability throughout the subsequent cycles.

6.3 Sensing Primitives

We investigated several methods of leveraging hollow alginate as sensors:

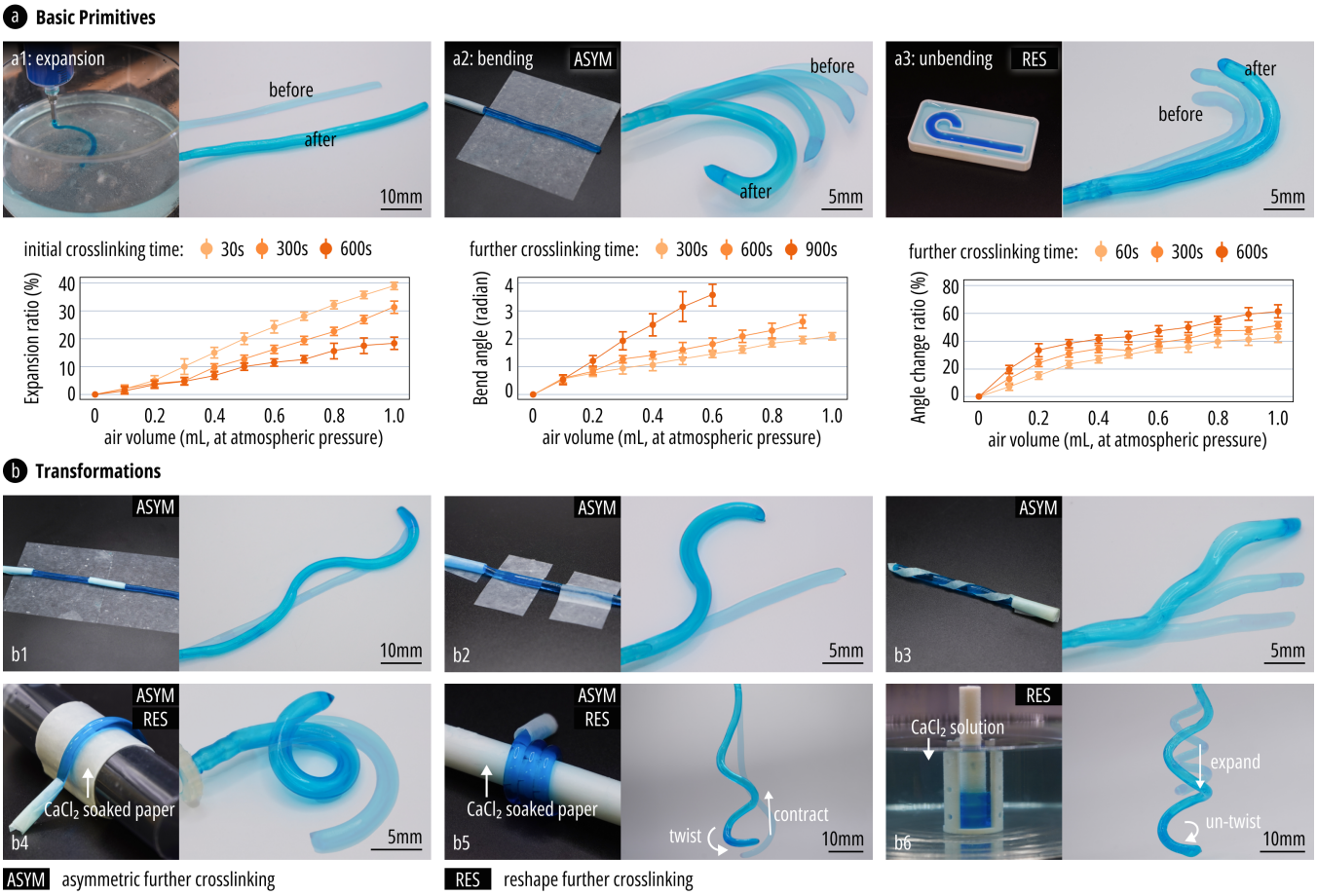

Figure 14: Morphing primitives of BioTube. Three basic primitives (a) can be combined to build complex transformations (b).

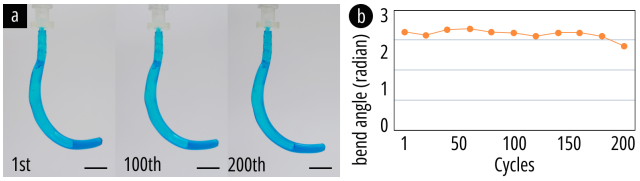

Figure 15: Repeatability test of the bending primitive (30-second initial crosslinking and 5-minute asymmetric crosslinking) over 200 cycles of inflation and deflation with 0.5mL of air of atmosphere pressure, after which the alginate fiber ruptured. (a) Images showing the fiber's maximum bend after inflation. (b) The maximum bend angle over the cycles.

6.3.1 Resistive stretch sensing. Utilizing $CaCl_2$ for ionic crosslinking, the presence of free Ca^{2+} and Cl^- ions impart ionic conductivity to the alginate [97], making it suitable for stretch sensing applications (Fig. 16 a). We compared 10-gauge needle extruded hollow alginate fibers (10-minute initial crosslinking) to solid alginate fibers (21-minute initial crosslinking) and tested five samples for each condition, calculating the average resistances under various strains (Fig. 16 a). The resistance was measured using a digital multimeter (FLUKE-87-5). The results showed that hollow alginate fibers exhibited slightly higher sensitivity to strain, similar to the findings from literature [22].

The increased sensitivity of the hollow fibers can be explained by the reduced cross-sectional area (S) compared to solid fibers. Under the same strain (i.e., with the same proportional change in length l), assuming the alginate volume remains constant, both hollow and solid fibers undergo similar proportional changes in S. However, because the hollow fibers have a smaller initial S, the change in $1/S$ is more pronounced, leading to a larger increase in resistance according to $R = \rho \frac{l}{S}$. This magnified change in resistance results in a higher sensitivity to strain in hollow fibers.

The hollow structure also increased the stretchability, aligning with observations from literature [22]. Because hollow fibers have a smaller cross-sectional area, there is less material resisting deformation, which results in less internal resistance to stretching compared to solid fibers. This reduced resistance allows hollow fibers to elongate further before breaking. As a result, all hollow

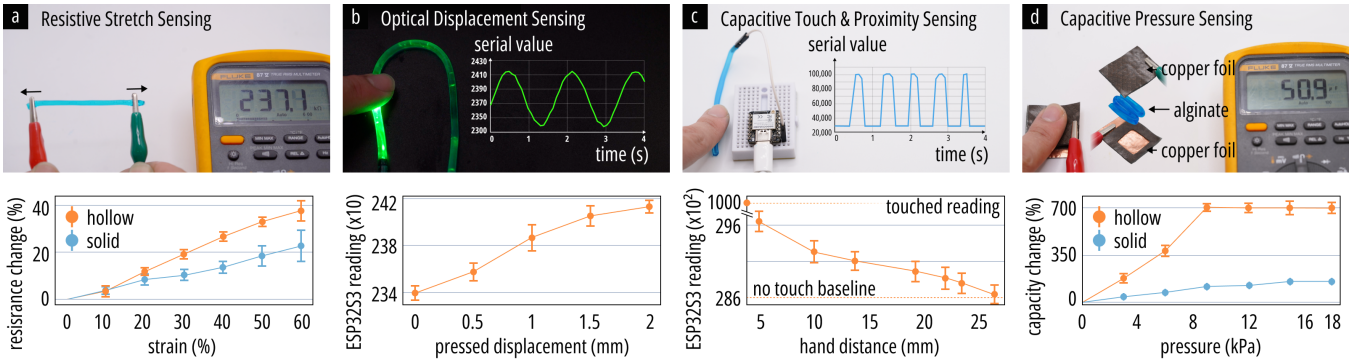

Figure 16: Sensing primitives of BioTube. (a) Resistive stretch sensing. (b) Optical displacement sensing. (c) Capacitive touch and proximity sensing. (d) Capacitive pressure sensing.

fibers withstood 70% of strain, while approximately half of the solid fibers ruptured between 60% and 70% of strain.

6.3.2 Optical displacement sensing. Hollow alginate fibers can also be used to transmit light through their channels. We 3D-printed an adapter similar to a luer hose barb, with one end connecting to a green laser pointer (Yiwu Zhangkun Electronic Commerce Co., Ltd) and the other inserted into the alginate fiber (Fig. 17 a). To prevent oil leakage, the connection between the alginate fiber and the laser pointer was sealed with plastic food wrap (Total Home). We tested different core materials—uncrosslinked alginate, air, tap water, and sunflower seed oil (365 by Whole Foods Market)—and found that sunflower oil provided the best light-conducting capability (Fig. 17, 180mm hollow alginate fiber with a 3-minute initial crosslinking was used, bent into a 180-degree shape). Sunflower oil's superior performance is likely due to its higher refractive index compared to the alginate shell, inducing total internal reflection inside the hollow fiber. Core materials were injected by cutting open one side of the fiber, removing the original core, and then injecting the desired medium. However, sharp bends or kinks should be avoided (Fig. 17 d2) as they allow light to escape.

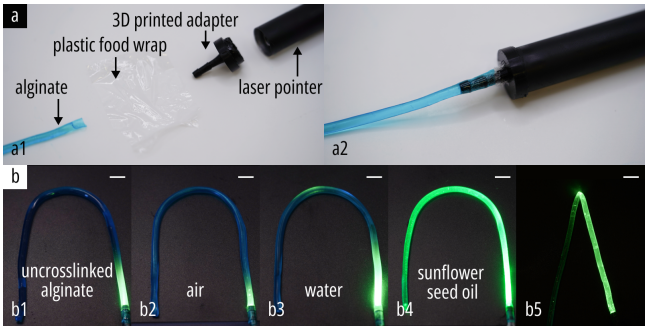

Figure 17: (a) Connection between the laser pointer and tubular hollow alginate. (b1-b4) Light-conducting performance of 180mm tubular hollow alginate (initially crosslinked for 3 minutes) with different core materials. (b5) Light transmission weakened by a sharp bend. (Scale bar: 10mm)

Leveraging this property, we developed an optical displacement-sensing fiber (Fig. 16 b). The same green laser was directed into the hollow alginate fiber, with a photoresistor (EBOOT) connected to the opposite end of the fiber using a 3D-printed housing to detect transmitted light. When the alginate fiber was pressed, the hollow channel became progressively obstructed, reducing laser transmission and producing a detectable signal change at the photoresistor. The STL files for all 3D-printed connector components are available in our GitHub repository[4].

The circuit consisted of a voltage divider with the photoresistor and a 10k resistor, and the voltage across the photoresistor was read by an analog pin on the ESP32S3 XIAO (Seeed Studio). Five alginate fiber samples (180 mm long with a 180-degree, 30-mm-radius bend at the center) were tested to obtain averaged signal responses under varying press distances (Fig. 16). The same pusher setup described in Section 5.2.3 was used, featuring a 2 cm-wide, circular 3D-printed tab to press the fiber's center. Exploring the optical displacement sensor as a pressure sensor could also be interesting, though we did not characterize the press displacement-force relationship of the alginate tube filled with sunflower oil in this work.

6.3.3 Capacitive touch and proximity sensing. Similar to other conductive interfaces [75, 89], ionically conductive alginate can be used for touch and proximity sensing via self-capacitance. When voltage is applied, the alginate and the Earth's surface form a capacitor, where the electric field is disturbed as body parts approach, allowing for the detection of proximity and touch events (Fig. 16 c). We inserted an M-to-M Dupont wire into the hollow alginate, with the other end connected to one built-in touch-sensing pin on ESP32S3 XIAO [5]. For proximity sensing, a hand was moved progressively closer to the alginate fiber (60mm in length), and for touch sensing, an index finger was used to make direct contact with the alginate. Five samples were tested to obtain averaged readings for both proximity and touch conditions. The results showed a clear increase in ESP readings as the hand approached the fiber, with a significantly higher signal when the alginate was touched, demonstrating the effectiveness of alginate-based proximity and touch sensors.

[4]https://github.com/biotube-alginate/pump/tree/main/model/optical
[5]ESP32S3 XIAO WiKi: https://wiki.seeedstudio.com/xiao_esp32s3_getting_started/

6.3.4 Capacitive pressure sensing. Hollow alginate can serve as a dielectric material in plate capacitors for pressure sensing (Fig. 16 d). We employed two 13 mm x 13 mm exposed copper foil areas (masked by insulation fabric) as electrodes, with alginate in the middle undergoing a 1-minute initial crosslinking, reshaping into an "M" shape, followed by 9 minutes of further reshaping crosslinking. Capacitance was measured using a digital multimeter (FLUKE-87-5), with five samples for each group tested to obtain averaged readings across various pressure levels.

This configuration demonstrated significantly higher pressure sensitivity compared to using solid alginate fibers as the dielectric, as hollow alginate deforms more under the same pressure, leading to greater changes in electrode distance, similar to findings in [15] where SLA-printed hollow structures were used as dielectric materials.

7 Applications

To further showcase the versatility of the BioTube, we ideated six transient use cases using tubular hollow alginate. Additionally, we visualized the corresponding crosslinking strategies (fabrication techniques) and functional primitives (achieved functionalities) for each application (Fig. 18).

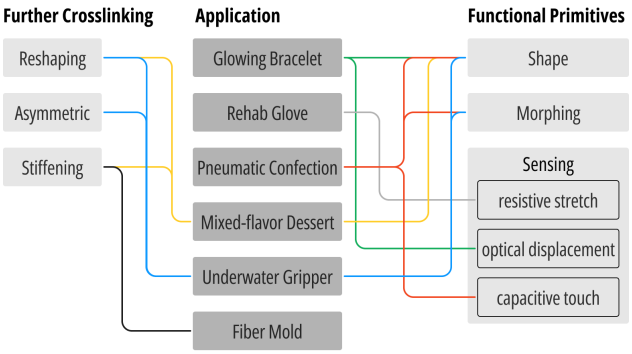

Figure 18: Summary of the further crosslinking strategies and functional primitives used for each application.

7.1 Eco-Friendly Glowing Bracelets

We designed an eco-friendly interactive glowing bracelet for concerts, live shows, and large gatherings like festivals or sports events. An 18 cm alginate fiber was initially crosslinked for 3 minutes, after which the core was removed with the roller method and refilled with sunflower seed oil. The hollow alginate served as a light-conducting fiber, utilizing the mechanism shown in (Fig. 16 c). When a pressing gesture was detected, the bracelet could switch between "always-on" and "flashing" light patterns (Fig. 19 a1, a2), offering a fun and interactive experience. More complex shape primitives, such as braiding (Fig. 19 a3), could also be incorporated, with one fiber strand used to conduct the light.

For the hardware (Fig. 19 b1), we modified a laser pointer as previously described, with an ESP32S3 XIAO as the processor, a photoresistor voltage-dividing circuit to detect light levels, a logic-level MOSFET (RFD14N05L) to control the laser's on/off state, and an additional vibration motor to provide haptic feedback upon detecting a press. The connection between the alginate fiber, laser pointer, and photoresistor (Fig. 19 b2, b3) followed the same setup as described in Section 6.3.2.

After the event, the bracelet can be buried in soil or composted (Fig. 19 c), as both the alginate and the sunflower seed oil are decomposable, while the hardware components are designed to be reusable and recyclable by event organizers.

We also conducted a preliminary evaluation of the bracelet's lifespan (Fig. 19 d). Initially, the laser illuminated the entire hollow alginate fiber, but light transmission gradually degraded over time. One possible cause is the gradual loss of water in the alginate shell, which might shift the refractive boundary conditions, reducing the efficiency of light transmission. The system continued to successfully detect press events at the 2-hour mark (Fig. 19 d4) but ceased to function after 3 hours.

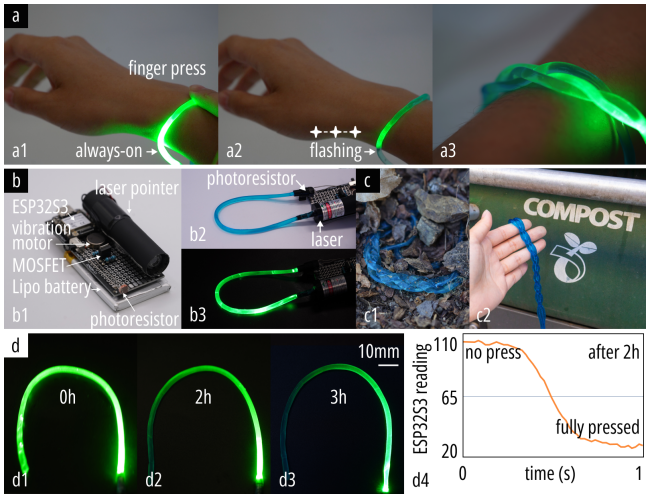

Figure 19: (a1, a2) The eco-friendly interactive glowing bracelet that changes light patterns when pressed. Alginate fibers were initially crosslinked for 3 minutes, after which the core was replaced with sunflower seed oil. (a3) Braided version of the bracelet. (b) Hardware components of the bracelet. (c) Disposal options for the alginate: burying in soil (c1) or discarding in a compost bin (c2). (d) Light transmission performance degradation of the alginate fiber over time, though it was still capable of sensing presses after 2 hours (d4).

7.2 Augmenting Gloves for Rehabilitation

BioTube can also temporarily augment off-the-shelf garments, such as gloves. We sewed hollow tubular alginate (initially crosslinked for 10 minutes, around 5cm) onto the central wrist area of a glove (Fig. 20 a1, a2) using conductive threads (Adafruit stainless thin conductive 2-ply thread), transforming it into a stretch-sensing wearable. Integrated into a voltage-dividing circuit (Fig. 20 a1), the alginate tube's resistance changes in response to stretching, enabling the monitoring of wrist movements. This augmented glove detects wrist flexion and extension, movements commonly used in

rehabilitation exercises for wrist fractures [66]. The same configuration can be applied to the side of the wrist (Fig. 20 b1) to sense radial and ulnar deviations, which are also key movements in wrist rehabilitation [66].

By detecting wrist movements, the glove can be used to control a game where the player navigates an object up and down to avoid obstacles (Fig. 20 a3) or moves a basket left and right to catch falling balls (Fig. 20 b2). This gamified rehabilitation transforms otherwise monotonous exercises into an interactive experience, with game design elements guiding the therapy process.

We conducted a preliminary lifespan and repeatability evaluation using hollow tubular alginate as stretch sensors, as shown in Figure 20 (a) (sensing wrist flexion and extension). Following the post-treatment method described in Section 5.3, we immersed the hollow tubular alginate in a glycerin-water (1:1) solution for 20 hours. Afterward, the alginate was sewn onto the central wrist area of the glove using conductive thread. On day 0, we performed 200 wrist flexion and extension cycles (approximately 2 seconds per cycle) to measure resistance changes at 90° and 0° wrist bends. The results indicated good stability over the cycles (Fig. 20 c). In the following four days, we tested the alginate fibers' response to wrist bend and found that although the baseline resistance shifted, the sensor still showed a considerable resistance change between 90° and 0° wrist bends (6.69% on day 4 compared to 18.11 wt.% on day 0, Fig. 20 d).

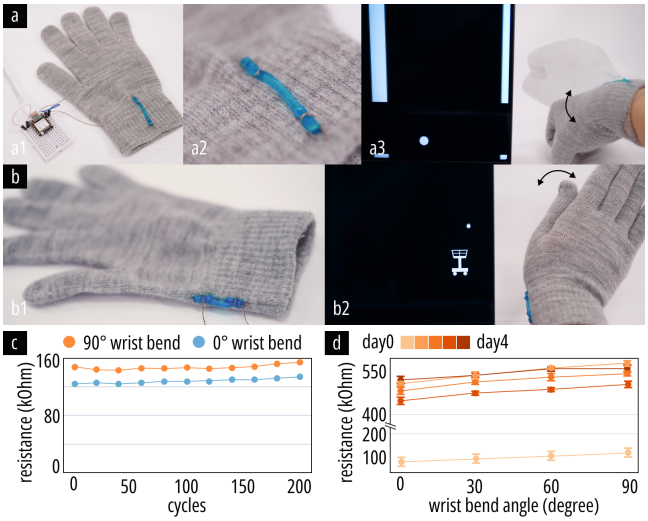

Figure 20: Glove with stretch-sensing capabilities for temporary wrist rehabilitation exercises. Alginate fibers were initially crosslinked for 10 minutes, the core was removed, and the fibers were sewn onto a glove using conductive threads. (a) The glove, with alginate fibers added to the central wrist area, senses wrist flexion and extension and is used to control an in-game object's movement to avoid obstacles. (b) With alginate fibers sewn onto the side of the wrist, the glove can also detect wrist radial and ulnar deviation, which can be used to move a basket in-game to catch falling balls. Repeatability (c) and lifespan (d) evaluation of the sensing capabilities of the glove (a) after post-processing the alginate with glycerin.

After rehabilitation, the alginate can easily detach and decompose, allowing the glove to return to its original form without any permanent modifications. We also envision these transient stretch sensors as valuable tools for prototype development, especially for short-term use or functional testing. Their temporary nature supports rapid iteration, testing, and eco-friendly disposal, offering a sustainable solution for early-stage designs.

7.3 Pneumatic Shape-Changing Dessert

The reshaping and morphing primitives of hollow tubular alginate opens up exciting possibilities in experimental gastronomy. To illustrate this, we created a confection called "*The Pulse of Valentine*" for Valentine's Day, featuring a heart-shaped alginate knot that, when touched, gently beats in sync with the giver's heartbeat.

The alginate fibers were initially crosslinked for 30 seconds, rinsed with tap water for 10 seconds, and knotted into a heart shape (Fig. 21 a1). Then, we used the syringe method described in Section 4.3.3 to remove the alginate core (Fig. 21 a2). Afterward, one end of the tube was sealed by tying a knot, while the other end was connected to a syringe pump and made contact with an Arduino pin for touch sensing. When touched, a low-pass filter connected via an Arduino pin detected the touch[6], and a pulse sensor (PulseSensor.com) captured the lover's heartbeat, triggering the modified syringe pump[7] to inflate and deflate the heart in rhythm with the pulse. A stepper motor (Usongshine Nema 17), paired with a TB6612 motor driver breakout board (Adafruit), drove the syringe pump using a rack-and-pinion mechanism.

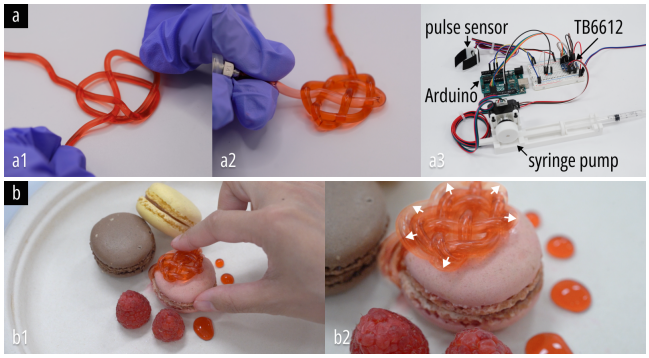

Figure 21: *The Pulse of Valentine*, a pneumatic shape-changing dessert for Valentine's Day. Alginate fibers were initially crosslinked for 30 seconds, tied into a heart knot (a1), and the core was removed by pumping air with a syringe (a2). The hollow alginate was then connected to a DIY syringe pump (a3), with hardware configured for pulse sensing, touch detection, and pump control. (b) When touched, the heart-shaped alginate knot inflates and deflates in rhythm with the detected pulse.

[6]https://playground.arduino.cc/Main/CapacitiveSensor/
[7]https://data.mrc.ox.ac.uk/data-set/syringe-pump

7.4 Spatially-Mixed Dual-Flavor Dessert

The hollow tubular alginate can enhance the culinary design process by incorporating multiple liquid-based flavors into a 3D structure. This approach eliminates the need for coagulants, traditionally required to stabilize fluid ingredients but often alter the original flavor.

We designed a dessert called *Winnie's Honey Pot*, featuring a spatially mixed dual flavor (Fig. 22). Alginate fibers were initially crosslinked for 10 seconds and then placed in a spiral mold for 3 minutes of further crosslinking (Fig. 22 a). After removing the core alginate, honey and lemon curd were injected into two hollow spiral alginate fibers (Fig. 22 b, c), which were then sealed by tying knots at the ends and subsequently stacked together. The stiffness of the alginate shell can be adjusted to create varying textural experiences, ranging from a soft, slow-release filling to a firmer, popping texture reminiscent of popping boba. We also envision that when connected to a syringe pump, these alginate tubes could serve as dynamic displays, dispensing sauces in real time to enhance interactivity and create a playful dining experience.

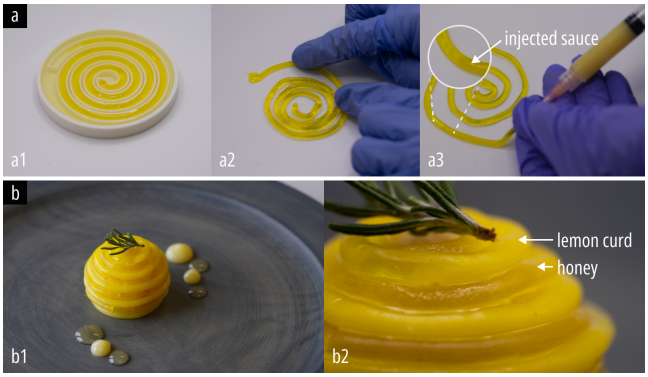

Figure 22: *Winnie's Honey Pot*, a dessert featuring spatially mixed dual flavors (b). Alginate fibers were initially crosslinked for 10 seconds, followed by 3 minutes of reshaping crosslinking in a spiral mold (a1). The core was then removed (a2) and filled with sauce (a3).

7.5 Biodegradable Underwater Grippers

Inspired by [92], we foresee the morphing capabilities of alginate being applied to underwater grippers, where the material can easily degrade in situ or be consumed by aquatic animals. To demonstrate this, we developed two types of grippers designed for retrieving underwater plastic waste (Fig. 23 a, b). In Section 6.2, we used air for actuation; here, we used water instead to prevent the alginate from floating.

The first gripper utilized the bending primitive (Fig. 14 a2). Alginate fiber, initially crosslinked for 30 seconds, underwent a 5-minute asymmetric further crosslinking induced by calcium-soaked paper. This gripper could hook onto latex waste (Fig. 23 a2) and lift it (Fig. 23 a3). Here, we demonstrate this single-bending actuator, which could only grab objects with a loop-like structure, allowing the actuator to insert into the loop, bend, and lift the object. We envision that multiple bending actuators could be connected to form a multi-fingered gripper, which can grasp objects with a wider range of geometries.

Figure 23: Biodegradable underwater grippers for plastic waste. Alginate fibers were initially crosslinked for 30 seconds, followed by 5 minutes of asymmetric crosslinking (a) and reshaping crosslinking (b). (a) Bending actuators designed to grip and lift loop-shaped latex waste. (b) Helical actuators capable of inserting into plastic bottles, expanding, and lifting them. (Scale bar: 10mm)

The second gripper was fabricated similarly to the method shown in Figure 14 b6. Alginate fiber, initially crosslinked for 30 seconds, was wrapped around an 8 mm diameter rod template and further crosslinked in the $CaCl_2$ solution for 5 minutes. This gripper was designed to insert into tubular structures and expand. For example, the helical structure could be inserted into a discarded water bottle (Fig. 23 b1), expand to grip the inner surface (Fig. 23 b2), and lift the bottle (Fig. 23 b3).

We could also make the gripper invisible by removing the dye in our material formula, which could potentially be less obtrusive to underwater creatures during operation [118]. Additionally, actuating the alginate with fluorescent liquids could mimic bioluminescent aquatic animals, helping the gripper blend into its surroundings or function as glow-in-the-dark biomimetic bait for attracting wildlife and delivering nutrition or vaccines [27].

7.6 Sacrificial Mold for Casting Elastomer Fibers

Inspired by [119], we fabricated elastomer fibers using hollow tubular alginate as sacrificial templates to cast elastomers with poor spinnability, such as silicones.

We mixed Ecoflex-30 with iron powder (1:1 w/w, DAILYLIFE) as the core elastomer for injection. For the alginate shell, we initially crosslinked the alginate fibers for 5 minutes, removed the core using the roller method, and then further crosslinked the hollow alginate in an 8 wt.% $CaCl_2$ solution for 10 minutes to stiffen the shell. The elastomer mixture was injected into the hollow alginate using a 14-gauge needle (Fig. 24 a1), and the fiber was then placed in boiling water for 20 minutes to cure the silicone (Fig. 24 a3). Afterward, the alginate shell was peeled off, revealing the magnetic elastomer fiber (Fig. 24 a4, a5).

We found that without stiffening crosslinking, the alginate shell was prone to leakage during injection (Fig. 24 a2), due to the high internal pressure created when injecting a viscous material like

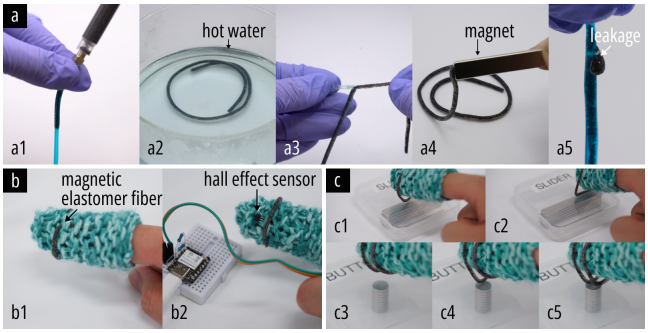

Figure 24: Using hollow tubular alginate as a sacrificial mold for casting magnetic elastomer fibers. Alginate fibers were initially crosslinked for 5 minutes, followed by a 5-minute stiffening crosslinking in 8 wt.% $CaCl_2$ solution to prevent leakage (a5). The magnetic elastomer mixture (1:1 Ecoflex-30 to iron powder) was then injected into the hollow alginate (a1), cured in hot water (a2), and the alginate shell was peeled away to retrieve the magnetic fiber. (b) Integration of the magnetic elastomer fiber into knitted textiles to provide haptic feedback, including damping (c1, c2) or a double-click effect (c3, c4, c5).

Ecoflex. Using our current method, we successfully fabricated magnetic elastomer fibers up to 30 cm in length (Fig. 24 a5). However, as discussed in Section 8.5, this injection method is unsuitable for casting extra-long fibers.

The magnetic elastomer fiber could be integrated into textiles by sewing it into a knitted finger-wear (Fig. 24 b1) to provide haptic feedback during interactions with passive, electronic-free magnetic interfaces (Fig. 24 c). A hall effect sensor (177119D) was incorporated to detect proximity to magnets (Fig. 24 b2). Three-dimensional magnetic sensors (e.g., TLV493D) could be used to detect finer relative positions between the finger and magnetic interfaces.

Leveraging silicone's high friction coefficient, we developed a slider with a damping haptic feedback. As the finger approaches the interface, the magnetic elastomer is attracted to the magnet. During linear movement, the elastomer is "dragged" along, generating resistance. Additionally, utilizing the fiber's elasticity, we created a mechanism that mimics double-click haptic feedback. Two magnetic fibers were integrated into the finger-wear, one with a thicker diameter (cast with an alginate template initially crosslinked for 3 minutes). The thinner fiber was attracted first, followed by the thicker one. When retracting, the thicker fiber stretched and snapped back first, followed by the thinner one, creating a double-click-like tactile feedback.

8 Discussions, Limitations, and Future Works

8.1 Towards Sustainability Beyond Waste Management

While Sustainable HCI currently focuses primarily on waste management [33], sustainability is, in fact, a multifaceted concept encompassing a wide range of goals across various domains [56, 67]. With BioTube, we aim to expand the toolkit for sustainable making practices within HCI by demonstrating its potential to be used in various transient devices, including actuators, sensors, fluid carriers, and more. Through these applications, we hope to contribute to the vision of fully biodegradable and transient systems [27].

We also envision that BioTube's versatility can inspire broader sustainability efforts beyond HCI. For instance, combined with their hollow structure and embedded conductive materials, they could serve as capacitive components for harvesting energy from microbes [120]. Additionally, they could aid in reforestation efforts with seeds embedded inside and leveraging the tunable slow-release properties of alginate [2]. Furthermore, BioTube could serve as temporary habitats for marine organisms, protecting their larval stage [45] and biodegrading as the organisms grow, thus contributing to biodiversity conservation.

By leveraging these envisioned diverse applications, BioTube can address multiple sustainability challenges beyond waste management, highlighting the importance of reimagining materials for a broader environmental impact. As we continue to explore innovative uses for BioTube, we anticipate their role in fostering more sustainable interactions among technology, humans, and nature, paving the way for a future where materials serve both human and ecological needs harmoniously.

Although we did not assess the biodegradability of hollow tubular alginate in this study, existing research provides useful insights. Sodium alginate has been shown to degrade by approximately 70% within 7 days [44], while crosslinked sodium alginate has been explored as a substitute for soil and as a plant growth substrate [84]. Glycerin, known as a degradable soil additive, enhances soil nutrient retention and supports healthy microbial growth [1]. Finally, sunflower oil, which can be degraded by soil microorganisms, improves the physicochemical properties of soil and promotes plant growth [123].

8.2 Using BioTube for FoodHCI

In this paper, we presented two applications where hollow tubular alginate was integrated into desserts, yet we foresee many more possibilities for BioTube in the field of FoodHCI [18]. For instance, BioTube could be used to create multi-channel food structures [19] that change flavors as diners consume them, or to create dynamic displays in food [21, 41], providing a more interactive and engaging dining experience. Although we did not explore applications for the capacitive pressure sensor (Fig. 16 d), it could be valuable for measuring the chewing force to control the user's eating habits [53].

Beyond HCI, BioTube could benefit cultured meat production by serving as a gel-based scaffold for 3D tissue formation [8, 37]. Its hollow structure could potentially enhance nutrient and oxygen distribution, supporting cell growth and enabling more structured cultured meat products.

8.3 Scalability of Hollow Fiber Production

While coaxial devices are capable of producing long hollow fibers through continuous spinning, a limitation of our fabrication process is the difficulty in creating continuous long fibers. Although this work does not focus on applications involving long hollow fibers, we explored a potential method to scale up our workflow for producing relatively long tubular hollow alginate fibers (Fig. 25). With the

syringe extrusion method, the extruded alginate fiber was guided through a water bath to remove excess calcium ions from its surface before being spooled onto a rod. In this setup, the spooler replaced the magnetic stirrer (as described in Section 4.2.1) as the drawing force. The spooling speed was carefully adjusted to synchronize with the extrusion speed, yielding an initial crosslinking time of approximately 3 minutes. The Hardware setup for this spooling system is detailed in our GitHub documentation[8]. We spooled a 148 cm alginate fiber and successfully removed its core using the roller method described in Section 4.3.3. However, we acknowledge that this method can be time-consuming and labor-intensive for longer fibers. Future work could explore a more automated core removal setup, potentially enabling on-the-fly core removal during alginate fiber extrusion.

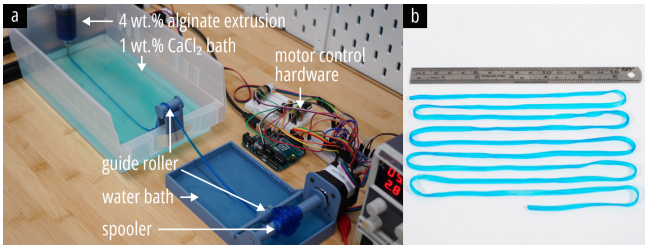

Figure 25: (a) Digital system for continuous alginate fiber crosslinking and spooling. (b) A 148 cm alginate fiber with its core removed using the roller method.

Moreover, while coaxial devices can produce microscale hollow fibers (e.g., in the micron range), our method faces limitations in achieving this scale. As shown in Figure 4 (a), alginate forms an immediate shell of approximately 0.4 mm upon contact with calcium ions. If the extrusion diameter is too small, the alginate will rapidly form a solid fiber, as demonstrated by the 22G and 24G needle extrusions in Figure 4 (c).

8.4 Alternative Initial Crosslinking Methods

In this work, we focused on extrusion-based fabrication methods for 1D fibers. However, other techniques could be explored for creating 2D or 3D geometries. For example, a CNC direct-write printer could extrude alginate onto a substrate, followed by immersion in a calcium solution for crosslinking. This method, however, may struggle to achieve a uniformly circular cross-section, as uncrosslinked alginate tends to flatten under gravity.

A mold-based approach, similar to plastic injection molding, could be used for 3D structures by injecting alginate into a mold with small holes for calcium ion penetration and crosslinking. Alternatively, embedded printing, as described in [112], could print alginate in a support bath, with calcium ions introduced later to initiate crosslinking.

8.5 Embedding Functional Materials

We could potentially cast fibers of other materials, such as liquid crystal elastomers, NIPAM hydrogel, and PDMS, using a method similar to that in Section 7.6. Leveraging the reshaping capabilities of alginate fibers, we can reshape the alginate before curing the inner material to create, for example, helical structures. Additionally, liquid metals could be embedded in alginate tubes and reshaped into solenoids, functioning as soft electromagnetic actuators, similar to [24], with a degradable shell and a reusable liquid metal core.

In this work, we did not characterize the inner surface of the alginate, which may have higher surface roughness than the outer surface due to shorter crosslinking time, making injection challenging. This issue could potentially be mitigated by immersing the entire alginate in a calcium solution until diffusion equilibrium is reached [102], as described in Section 7.6. There, we also used a higher-concentration calcium solution to increase the shell's mechanical strength and prevent rupture. However, it is important to note that the injection method is unsuitable for casting continuously long fibers, as injection friction increases with fiber length. As reported in Section 7.6, we were only able to fabricate magnetic elastomer fibers up to 30 cm.

8.6 Morphing Alginate as Actuators

In Section 6.2, we demonstrated the morphing capabilities of hollow tubular alginate, and in Section 7.5, we further showcased how these morphing capabilities could be leveraged for actuation. However, the load-bearing capacity of a single alginate fiber remained limited. In Figure 23 (a), the net weight (excluding buoyant force) of the latex waste was approximately 0.002N, while in Figure 23 (b), the net weight of the bottle was around 0.04N. This gentle gripping nature shows promise in handling delicate objects such as small insects or aquatic organisms if manufactured on a smaller scale, for example, by extruding the alginate fiber with a larger gauge needle for initial crosslinking. The low-exerted force could also be beneficial in microsurgery, such as in endovascular procedures, with the biocompatibility of alginate further enhancing its suitability for medical applications.

To generate a larger actuation force, a potential improvement could involve combining multiple morphing alginate fibers to increase the overall actuation force. For instance, deploying several helical actuators simultaneously or integrating multiple bending actuators in a woven structure could enhance performance. We also plan to explore additional applications for these morphing alginate fibers, such as developing crawling or swimming robots.

9 Conclusion

In this work, we present BioTube, a DIY-friendly and sustainable fabrication method for producing hollow tubular alginate structures. We first investigated and quantified the progressive crosslinking process, including initial crosslinking and three further crosslinking techniques: reshaping, asymmetric, and stiffening crosslinking. We also evaluated a post-treatment process to extend the lifespan of the alginate. These techniques allow for customization of various parameters, such as diameter, shell thickness, shape, cross-sectional profile, stiffness, and shelf-life.

We then explored three functional primitives of hollow tubular alginate: (1) shape, which includes reshaping crosslinking-based forms and thread-based shaping techniques; (2) morphing, achieved through reshaping and asymmetric crosslinking to enable inflation

[8]https://github.com/biotube-alginate/pump/tree/main

with air or water; and (3) sensing, which covers resistive stretch sensing, optical displacement sensing, and capacitive touch, proximity, and pressure sensing.

Finally, we explored the application space of hollow tubular alginate for creating transient devices, ranging from wearables with embedded sensing capabilities to experimental gastronomy. With BioTube, we aim to enrich the sustainable-making toolkit, inspiring designers, makers, and researchers to innovate and create within the growing field of sustainable design.

Acknowledgments

The authors acknowledge support from the National Science Foundation Grant CAREER-2427455, 2427553, and 2427457. The authors also sincerely thank the reviewers for their valuable and constructive feedback, with special appreciation to Danchang Yan for her contributions in designing and providing insightful feedback on several illustrations, and to Hajun Lee for his advice and assistance with our experiments.

References

[1] Carmen Betancourt Aguilar, Renato de Mello Prado, Leónides Castellanos Gonzáles, and Cid N Silva Campos. 2016. Glycerin as byproduct of biodiesel production, its characteristics, applications and soil use. *Cultivos Tropicales* 37, 3 (2016), 7–14. https://doi.org/10.13140/RG.2.1.4329.2403

[2] Esraa G. Arafa, Magdy W. Sabaa, Riham R. Mohamed, Ali M. Elzanaty, and Omayma F. Abdel-Gawad. 2022. Preparation of biodegradable sodium alginate/carboxymethylchitosan hydrogels for the slow-release of urea fertilizer and their antimicrobial activity. *Reactive and Functional Polymers* 174 (May 2022), 105243. https://doi.org/10.1016/j.reactfunctpolym.2022.105243

[3] Fiona Bell, Latifa Al Naimi, Ella McQuaid, and Mirela Alistar. 2022. Designing with Alganyl. In *Proceedings of the Sixteenth International Conference on Tangible, Embedded, and Embodied Interaction* (Daejeon, Republic of Korea) *(TEI '22)*. Association for Computing Machinery, New York, NY, USA, Article 2, 14 pages. https://doi.org/10.1145/3490149.3501308

[4] Fiona Bell, Derrek Chow, Hyelin Choi, and Mirela Alistar. 2023. SCOBY BREASTPLATE: SLOWLY GROWING A MICROBIAL INTERFACE. In *Proceedings of the Seventeenth International Conference on Tangible, Embedded, and Embodied Interaction* (Warsaw, Poland) *(TEI '23)*. Association for Computing Machinery, New York, NY, USA, Article 34, 15 pages. https://doi.org/10.1145/3569009.3572805

[5] Fiona Bell, Netta Ofer, and Mirela Alistar. 2022. ReClaym our Compost: Biodegradable Clay for Intimate Making. In *Proceedings of the 2022 CHI Conference on Human Factors in Computing Systems* (New Orleans, LA, USA) *(CHI '22)*. Association for Computing Machinery, New York, NY, USA, Article 454, 15 pages. https://doi.org/10.1145/3491102.3517711

[6] Eli Blevis. 2007. Sustainable interaction design: invention & disposal, renewal & reuse. In *Proceedings of the SIGCHI Conference on Human Factors in Computing Systems* (San Jose, California, USA) *(CHI '07)*. Association for Computing Machinery, New York, NY, USA, 503–512. https://doi.org/10.1145/1240624.1240705

[7] Modernist Pantry Blog. 2024. Lesson 1: Direct Spherification. https://blog.modernistpantry.com/spherification-course/lesson-1-direct-spherification-2/. Accessed: 2024-08-11.

[8] Claire Bomkamp, Stacey C. Skaalure, Gonçalo F. Fernando, Tom Ben-Arye, Elliot W. Swartz, and Elizabeth A. Specht. 2022. Scaffolding Biomaterials for 3D Cultivated Meat: Prospects and Challenges. *Advanced Science* 9, 3 (2022), 2102908. https://doi.org/10.1002/advs.202102908 arXiv:https://onlinelibrary.wiley.com/doi/pdf/10.1002/advs.202102908

[9] Leah Buechley and Ruby Ta. 2023. 3D Printable Play-Dough: New Biodegradable Materials and Creative Possibilities for Digital Fabrication. In *Proceedings of the 2023 CHI Conference on Human Factors in Computing Systems* (Hamburg, Germany) *(CHI '23)*. Association for Computing Machinery, New York, NY, USA, Article 850, 15 pages. https://doi.org/10.1145/3544548.3580813

[10] Lianqi Cao, Wei Lu, Analucia Mata, Katsuyoshi Nishinari, and Yapeng Fang. 2020. Egg-box model-based gelation of alginate and pectin: A review. *Carbohydrate polymers* 242 (2020), 116389. https://doi.org/10.1016/j.carbpol.2020.116389

[11] Lai Wah Chan, Huey Ying Lee, and Paul WS Heng. 2006. Mechanisms of external and internal gelation and their impact on the functions of alginate as a coat and delivery system. *Carbohydrate Polymers* 63, 2 (2006), 176–187. https://doi.org/10.1016/j.carbpol.2005.07.033

[12] Tingyu Cheng, Taylor Tabb, Jung Wook Park, Eric M Gallo, Aditi Maheshwari, Gregory D. Abowd, Hyunjoo Oh, and Andreea Danielescu. 2023. Functional Destruction: Utilizing Sustainable Materials' Physical Transiency for Electronics Applications. In *Proceedings of the 2023 CHI Conference on Human Factors in Computing Systems* (Hamburg, Germany) *(CHI '23)*. Association for Computing Machinery, New York, NY, USA, Article 366, 16 pages. https://doi.org/10.1145/3544548.3580811

[13] Yao Cheng, Fuyin Zheng, Jie Lu, Luoran Shang, Zhuoying Xie, Yuanjin Zhao, Yongping Chen, and Zhongze Gu. 2014. Bioinspired multicompartmental microfibers from microfluidics. *Advanced materials (Deerfield Beach, Fla.)* 26, 30 (2014), 5184–5190. https://doi.org/10.1002/adma.201400798

[14] Kyung Yun Choi and Hiroshi Ishii. 2021. Therms-Up!: DIY Inflatables and Interactive Materials by Upcycling Wasted Thermoplastic Bags. In *Proceedings of the Fifteenth International Conference on Tangible, Embedded, and Embodied Interaction* (Salzburg, Austria) *(TEI '21)*. Association for Computing Machinery, New York, NY, USA, Article 51, 8 pages. https://doi.org/10.1145/3430524.3442457

[15] Ziying Cui, Shaojie Cao, Chen Huang, Yufan Chen, Mengdan Zhang, Ao Wang, and Xueliang Xiao. 2024. Broad detection range of flexible capacitive sensor with 3D printed interwoven hollow dual-structured dielectric layer. *Applied Materials Today* 36 (2024), 102064. https://doi.org/10.1016/j.apmt.2024.102064

[16] Dr. D-Flo. 2017. DIY Syringe Pump Project. https://www.drdflo.com/pages/Projects/Syringe-Pump.html Accessed: 2024-12-07.

[17] Karijn Den Teuling, Amy Winters, and Miguel Bruns. 2024. Chitosan Biofilm Actuators: Humidity Responsive Materials for Sustainable Interaction Design. In *Proceedings of the Eighteenth International Conference on Tangible, Embedded, and Embodied Interaction* (Cork, Ireland) *(TEI '24)*. Association for Computing Machinery, New York, NY, USA, Article 81, 7 pages. https://doi.org/10.1145/3623509.3635262

[18] Jialin Deng, Ferran Altarriba Bertran, Lining Yao, Marianna Obrist, Koya Narumi, Humphrey Yang, Mako Miyatake, and Florian Mueller. 2022. Mapping FoodHCI Futures. In *Extended Abstracts of the 2022 CHI Conference on Human Factors in Computing Systems* (New Orleans, LA, USA) *(CHI EA '22)*. Association for Computing Machinery, New York, NY, USA, Article 166, 5 pages. https://doi.org/10.1145/3491101.3516401

[19] Jialin Deng and Florian 'Floyd' Mueller. 2023. The "Logic Bonbon": A Computable Food, Or an Eatable Computer?. In *Companion Publication of the 2023 ACM Designing Interactive Systems Conference* (Pittsburgh, PA, USA) *(DIS '23 Companion)*. Association for Computing Machinery, New York, NY, USA, 77–80. https://doi.org/10.1145/3563703.3596646

[20] Jialin Deng, Patrick Olivier, Josh Andres, Kirsten Ellis, Ryan Wee, and Florian Floyd Mueller. 2022. Logic Bonbon: Exploring Food as Computational Artifact. In *Proceedings of the 2022 CHI Conference on Human Factors in Computing Systems* (New Orleans, LA, USA) *(CHI '22)*. Association for Computing Machinery, New York, NY, USA, Article 47, 21 pages. https://doi.org/10.1145/3491102.3501926

[21] Jialin Deng, Humphrey Yang, Aryan Saini, Urs Dominic Gaudenz, Lining Yao, Patrick Olivier, and Florian 'Floyd' Mueller. 2023. Dancing Delicacies: Designing Computational Food for Dynamic Dining Trajectories. In *Proceedings of the 2023 ACM Designing Interactive Systems Conference* (Pittsburgh, PA, USA) *(DIS '23)*. Association for Computing Machinery, New York, NY, USA, 244–262. https://doi.org/10.1145/3563657.3596021

[22] Pengfei Deng, Zijian He, Yingnan Shen, Noor Mohammad Mohammad, Wenhui Xu, Bumsoo Han, and Tian Li. 2024. Conductive hollow hydrogel fibers toward high-sensitivity bio-textiles. *Cell Reports Physical Science* 5, 7 (2024), 102047. https://doi.org/10.1016/j.xcrp.2024.102047

[23] Kristin N. Dew and Daniela K. Rosner. 2019. Designing with Waste: A Situated Inquiry into the Material Excess of Making. In *Proceedings of the 2019 on Designing Interactive Systems Conference* (San Diego, CA, USA) *(DIS '19)*. Association for Computing Machinery, New York, NY, USA, 1307–1319. https://doi.org/10.1145/3322276.3322320

[24] Thanh Nho Do, Hung Phan, Thuc-Quyen Nguyen, and Yon Visell. 2018. Miniature soft electromagnetic actuators for robotic applications. *Advanced Functional Materials* 28, 18 (2018), 1800244. https://doi.org/10.1002/adfm.201800244

[25] Andrea Dodero, Silvia Vicini, Marina Alloisio, and Maila Castellano. 2019. Sodium alginate solutions: Correlation between rheological properties and spinnability. *Journal of materials science* 54, 10 (2019), 8034–8046. https://doi.org/10.1007/s10853-019-03446-3

[26] Xiang-Yun Du, Qing Li, Guan Wu, and Su Chen. 2019. Multifunctional micro/nanoscale fibers based on microfluidic spinning technology. *Advanced Materials* 31, 52 (2019), 1903733. https://doi.org/10.1002/adma.201903733

[27] Dario Floreano, Bokeon Kwak, Markéta Pankhurst, Jun Shintake, Mario Caironi, Valerio F Annese, Qiukai Qi, Jonathan Rossiter, and Remko M Boom. 2024. Towards edible robots and robotic food. *Nature Reviews Materials* 9, 8 (August 2024), 589–599. https://doi.org/10.1038/s41578-024-00688-9

[28] Qing Gao, Yong He, Jian-zhong Fu, An Liu, and Liang Ma. 2015. Coaxial nozzle-assisted 3D bioprinting with built-in microchannels for nutrients delivery. *Biomaterials* 61 (2015), 203–215. https://doi.org/10.1016/j.biomaterials.2015.05.031

[29] Qing Gao, Zhenjie Liu, Zhiwei Lin, Jingjiang Qiu, Yu Liu, An Liu, Yidong Wang, Meixiang Xiang, Bing Chen, Jianzhong Fu, et al. 2017. 3D bioprinting of vessel-like structures with multilevel fluidic channels. *ACS biomaterials science & engineering* 3, 3 (2017), 399–408. https://doi.org/10.1021/acsbiomaterials.6b00643

[30] Çağlar Genç, Emilia Launne, and Jonna Häkkilä. 2022. Interactive Mycelium Composites: Material Exploration on Combining Mushroom with Off-the-shelf Electronic Components. In *Nordic Human-Computer Interaction Conference* (Aarhus, Denmark) *(NordiCHI '22)*. Association for Computing Machinery, New York, NY, USA, Article 19, 12 pages. https://doi.org/10.1145/3546155.3546689

[31] Atabak Ghanizadeh Tabriz, Christopher G Mills, John J Mullins, Jamie A Davies, and Wenmiao Shu. 2017. Rapid fabrication of cell-laden alginate hydrogel 3D structures by micro dip-coating. *Frontiers in Bioengineering and Biotechnology* 5 (2017), 13. https://doi.org/10.3389/fbioe.2017.00013

[32] Wei Huang Goh and Michinao Hashimoto. 2018. Dual sacrificial molding: Fabricating 3D microchannels with overhang and helical features. *Micromachines* 9, 10 (2018), 523. https://doi.org/10.3390/mi9100523

[33] Lon Åke Erni Johannes Hansson, Teresa Cerratto Pargman, and Daniel Sapiens Pargman. 2021. A Decade of Sustainable HCI: Connecting SHCI to the Sustainable Development Goals. In *Proceedings of the 2021 CHI Conference on Human Factors in Computing Systems* (Yokohama, Japan,) *(CHI '21)*. Association for Computing Machinery, New York, NY, USA, Article 300, 19 pages. https://doi.org/10.1145/3411764.3445069

[34] Liang He, Gierad Laput, Eric Brockmeyer, and Jon E. Froehlich. 2017. SqueezaPulse: Adding Interactive Input to Fabricated Objects Using Corrugated Tubes and Air Pulses. In *Proceedings of the Eleventh International Conference on Tangible, Embedded, and Embodied Interaction* (Yokohama, Japan) *(TEI '17)*. Association for Computing Machinery, New York, NY, USA, 341–350. https://doi.org/10.1145/3024969.3024976

[35] Kayoko Hirayama, Hiroaki Onoe, and Shoji Takeuchi. 2012. 3D microfluidics formed with hydrogel sacrificial structures. In *2012 IEEE 25th International Conference on Micro Electro Mechanical Systems (MEMS)*. IEEE, IEEE, Paris, France, 200–203. https://doi.org/10.1109/MEMSYS.2012.6170125

[36] Min Hu, Rensheng Deng, Karl M Schumacher, Motoichi Kurisawa, Hongye Ye, Kristy Purnamawati, and Jackie Y Ying. 2010. Hydrodynamic spinning of hydrogel fibers. *Biomaterials* 31, 5 (2010), 863–869. https://doi.org/10.1016/j.biomaterials.2009.10.002

[37] Byeongwook Jo, Minghao Nie, and Shoji Takeuchi. 2021. Manufacturing of animal products by the assembly of microfabricated tissues. *Essays in Biochemistry* 65, 3 (08 2021), 611–623. https://doi.org/10.1042/EBC20200092 arXiv:https://portlandpress.com/essaysbiochem/article-pdf/65/3/611/918421/ebc-2020-0092c.pdf

[38] Trevor J Jones, Etienne Jambon-Puillet, Joel Marthelot, and P-T Brun. 2021. Bubble casting soft robotics. *Nature* 599, 7884 (2021), 229–233. https://doi.org/10.1038/s41586-021-04029-6

[39] J.R. Wagner Jr., E.M. Mount III, and H.F. Giles Jr. 2014. *Extrusion: The Definitive Processing Guide and Handbook* (2nd ed.). William Andrew Publishing, Oxford. 620 pages. https://books.google.com/books?hl=en&lr=&id=kGBkwC4akrsC

[40] Georgia Kaklamani, David Cheneler, Liam M Grover, Michael J Adams, and James Bowen. 2014. Mechanical properties of alginate hydrogels manufactured using external gelation. *Journal of the mechanical behavior of biomedical materials* 36 (2014), 135–142. https://doi.org/10.1016/j.jmbbm.2014.04.013

[41] Viirj Kan, Emma Vargo, Noa Machover, Hiroshi Ishii, Serena Pan, Weixuan Chen, and Yasuaki Kakehi. 2017. Organic Primitives: Synthesis and Design of pH-Reactive Materials using Molecular I/O for Sensing, Actuation, and Interaction. In *Proceedings of the 2017 CHI Conference on Human Factors in Computing Systems* (Denver, Colorado, USA) *(CHI '17)*. Association for Computing Machinery, New York, NY, USA, 989–1000. https://doi.org/10.1145/3025453.3025952

[42] Ozgun Kilic Afsar, Ali Shtarbanov, Hila Mor, Ken Nakagaki, Jack Forman, Karen Modrei, Seung Hee Jeong, Klas Hjort, Kristina Höök, and Hiroshi Ishii. 2021. OmniFiber: Integrated Fluidic Fiber Actuators for Weaving Movement based Interactions into the 'Fabric of Everyday Life'. In *The 34th Annual ACM Symposium on User Interface Software and Technology* (Virtual Event, USA) *(UIST '21)*. Association for Computing Machinery, New York, NY, USA, 1010–1026. https://doi.org/10.1145/3472749.3474802

[43] Marion Koelle, Madalina Nicolae, Aditya Shekhar Nittala, Marc Teyssier, and Jürgen Steimle. 2022. Prototyping Soft Devices with Interactive Bioplastics. In *Proceedings of the 35th Annual ACM Symposium on User Interface Software and Technology* (Bend, OR, USA) *(UIST '22)*. Association for Computing Machinery, New York, NY, USA, Article 19, 16 pages. https://doi.org/10.1145/3526113.3545623

[44] Jagoda Kurowiak, Agnieszka Mackiewicz, Tomasz Klekiel, and Romuald Będziński. 2022. Evaluation of selected properties of sodium alginate-based hydrogel material—Mechanical strength, μDIC analysis and degradation. *Materials* 15, 3 (2022), 1225. https://doi.org/10.3390/ma15031225

[45] Inyeong Kwon, Kyounghoon Lee, and Taeho Kim. 2019. Shelter material and shape preferences of the sea cucumber, Apostichopus japonicus. *Aquaculture* 508 (2019), 206–213. https://doi.org/10.1016/j.aquaculture.2019.05.011

[46] Eldy S. Lazaro Vasquez, Mirela Alistar, Laura Devendorf, and Michael L. Rivera. 2024. Desktop Biofibers Spinning: An Open-Source Machine for Exploring Biobased Fibers and Their Application Towards Sustainable Smart Textile Design. In *Proceedings of the CHI Conference on Human Factors in Computing Systems* (Honolulu, HI, USA) *(CHI '24)*. Association for Computing Machinery, New York, NY, USA, Article 856, 18 pages. https://doi.org/10.1145/3613904.3642387

[47] Eldy S. Lazaro Vasquez, Netta Ofer, Shanel Wu, Mary Etta West, Mirela Alistar, and Laura Devendorf. 2022. Exploring Biofoam as a Material for Tangible Interaction. In *Proceedings of the 2022 ACM Designing Interactive Systems Conference* (Virtual Event, Australia) *(DIS '22)*. Association for Computing Machinery, New York, NY, USA, 1525–1539. https://doi.org/10.1145/3532106.3533494

[48] Kwang Ho Lee, Su Jung Shin, Yongdoo Park, and Sang Hoon Lee. 2009. Synthesis of cell-laden alginate hollow fibers using microfluidic chips and microvascularized tissue-engineering applications. *small* 5, 11 (2009), 1264–1268. https://doi.org/10.1002/smll.200801667

[49] P Lee and MA Rogers. 2012. Effect of calcium source and exposure-time on basic caviar spherification using sodium alginate. *International Journal of Gastronomy and Food Science* 1, 2 (2012), 96–100. https://doi.org/10.1016/j.ijgfs.2013.06.003

[50] Jiwei Li, Yadong Wu, Jinmei He, and Yudong Huang. 2016. A new insight to the effect of calcium concentration on gelation process and physical properties of alginate films. *Journal of Materials Science* 51 (2016), 5791–5801. https://doi.org/10.1007/s10853-016-9880-0

[51] Shuai Li, Kan Wang, Xuzhou Jiang, Qingxi Hu, Chuck Zhang, and Ben Wang. 2020. Rapid Fabrication of Ready-to-Use Gelatin Scaffolds with Prevascular Networks Using Alginate Hollow Fibers as Sacrificial Templates. *ACS Biomaterials Science & Engineering* 6, 4 (2020), 2297–2311. https://doi.org/10.1021/acsbiomaterials.9b01834 arXiv:https://doi.org/10.1021/acsbiomaterials.9b01834 PMID: 33455307.

[52] Y Li, Y Liu, C Jiang, S Li, G Liang, and Q Hu. 2016. A reactor-like spinneret used in 3D printing alginate hollow fiber: a numerical study of morphological evolution. *Soft Matter* 12, 8 (2016), 2392–2399. https://doi.org/10.1039/C5SM02733K

[53] Ying-Ju Lin, Parinya Punpongsanon, Xin Wen, Daisuke Iwai, Kosuke Sato, Marianna Obrist, and Stefanie Mueller. 2020. FoodFab: Creating Food Perception Illusions using Food 3D Printing. In *Proceedings of the 2020 CHI Conference on Human Factors in Computing Systems* (Honolulu, HI, USA) *(CHI '20)*. Association for Computing Machinery, New York, NY, USA, 1–13. https://doi.org/10.1145/3313831.3376421

[54] Guanhong Liu, Haiqing Xu, Xianghua(Sharon) Ding, Mingyue Gao, Bowen Li, Fushen Ruan, and Haipeng Mi. 2022. "It Puts Life into My Creations": Understanding Fluid Fiber as a Media for Expressive Display. In *Proceedings of the 2022 CHI Conference on Human Factors in Computing Systems* (New Orleans, LA, USA) *(CHI '22)*. Association for Computing Machinery, New York, NY, USA, Article 49, 15 pages. https://doi.org/10.1145/3491102.3501990

[55] XD Liu, WY Yu, Y Zhang, WM Xue, WT Yu, Y Xiong, XJ Ma, Y Chen, and Q Yuan. 2002. Characterization of structure and diffusion behaviour of Ca-alginate beads prepared with external or internal calcium sources. *Journal of microencapsulation* 19, 6 (2002), 775–782. https://doi.org/10.1080/0265204021000022743

[56] Qiuyu Lu, Andreea Danielescu, Vikram Iyer, Pedro Lopes, and Lining Yao. 2024. Ecological HCI: Reflection and Future. In *Extended Abstracts of the CHI Conference on Human Factors in Computing Systems* (Honolulu, HI, USA) *(CHI EA '24)*. Association for Computing Machinery, New York, NY, USA, Article 577, 4 pages. https://doi.org/10.1145/3613905.3643985

[57] Qiuyu Lu, Jifei Ou, João Wilbert, André Haben, Haipeng Mi, and Hiroshi Ishii. 2019. milliMorph – Fluid-Driven Thin Film Shape-Change Materials for Interaction Design. In *Proceedings of the 32nd Annual ACM Symposium on User Interface Software and Technology* (New Orleans, LA, USA) *(UIST '19)*. Association for Computing Machinery, New York, NY, USA, 663–672. https://doi.org/10.1145/3332165.3347956

[58] Qiuyu Lu, Semina Yi, Mengtian Gan, Jihong Huang, Xiao Zhang, Yue Yang, Chenyi Shen, and Lining Yao. 2024. Degrade to Function: Towards Eco-friendly Morphing Devices that Function Through Programmed Sequential Degradation. In *Proceedings of the 37th Annual ACM Symposium on User Interface Software and Technology* (Pittsburgh, PA, USA) *(UIST '24)*. Association for Computing Machinery, New York, NY, USA, 24 pages. https://doi.org/10.1145/3654777.3676464

[59] Qiuyu Lu, Tianyu Yu, Semina Yi, Yuran Ding, Haipeng Mi, and Lining Yao. 2023. Sustainflatable: Harvesting, Storing and Utilizing Ambient Energy for Pneumatic Morphing Interfaces. In *Proceedings of the 36th Annual ACM Symposium on User Interface Software and Technology* (San Francisco, CA, USA) *(UIST '23)*. Association for Computing Machinery, New York, NY, USA, Article 32, 20 pages. https://doi.org/10.1145/3586183.3606721

[60] Danli Luo, Jianzhe Gu, Fang Qin, Guanyun Wang, and Lining Yao. 2020. E-seed: Shape-Changing Interfaces that Self Drill. In *Proceedings of the 33rd Annual ACM Symposium on User Interface Software and Technology* (Virtual Event, USA) *(UIST '20)*. Association for Computing Machinery, New York, NY, USA, 45–57. https://doi.org/10.1145/3379337.3415855

[61] Yongxiang Luo, Birui Chen, Xiaonan Zhang, Shuai Huang, and Qingde Wa. 2022. 3D printed concentrated alginate/GelMA hollow-fibers-packed scaffolds with nano apatite coatings for bone tissue engineering. *International Journal of Biological Macromolecules* 202 (2022), 366–374. https://doi.org/10.1016/j.

ijbiomac.2022.01.096

[62] Bruna Maciel, Claude Oelschlaeger, and Norbert Willenbacher. 2020. Chain flexibility and dynamics of alginate solutions in different solvents. *Colloid and Polymer Science* 298 (2020), 791–801. https://doi.org/10.1007/s00396-020-04612-9

[63] Ramses V Martinez, Carina R Fish, Xin Chen, and George M Whitesides. 2012. Elastomeric origami: programmable paper-elastomer composites as pneumatic actuators. *Advanced functional materials* 22, 7 (2012), 1376–1384. https://doi.org/10.1002/adfm.201102978

[64] Ken Matsubara and Hiroki Ota. 2019. Stretchable liquid metal wiring with three-dimentional helical structure. In *2019 IEEE 32nd International Conference on Micro Electro Mechanical Systems (MEMS)*. IEEE, IEEE, Seoul, Korea (South), 296–298. https://doi.org/10.1109/MEMSYS.2019.8870779

[65] Zhi-Jun Meng, Wei Wang, Rui Xie, Xiao-Jie Ju, Zhuang Liu, and Liang-Yin Chu. 2016. Microfluidic generation of hollow Ca-alginate microfibers. *Lab on a Chip* 16, 14 (2016), 2673–2681. https://doi.org/10.1039/c6lc00640j

[66] MyHealth.Alberta.ca. 2024. Wrist Fracture: Rehab Exercises. https://myhealth.alberta.ca/Health/aftercareinformation/pages/conditions.aspx?hwid=bo1655. Accessed: 2024-09-06.

[67] United Nations. 2023. Take Action for the Sustainable Development Goals. https://www.un.org/sustainabledevelopment/sustainable-development-goals/. Accessed: Dec 10, 2023.

[68] Audrey Ng. 2017. Grown microbial 3D fiber art, Ava: fusion of traditional art with technology. In *Proceedings of the 2017 ACM International Symposium on Wearable Computers* (Maui, Hawaii) *(ISWC '17)*. Association for Computing Machinery, New York, NY, USA, 209–214. https://doi.org/10.1145/3123021.3123069

[69] Thi Phuong Thuy Nguyen, Buu Minh Tran, and Nae Yoon Lee. 2018. Microfluidic approach for the fabrication of cell-laden hollow fibers for endothelial barrier research. *Journal of Materials Chemistry B* 6, 38 (2018), 6057–6066. https://doi.org/10.1039/C8TB02031K

[70] Madalina Nicolae, Claire Lefez, Anne Roudaut, Samuel Huron, Jürgen Steimle, and Marc Teyssier. 2024. SoftBioMorph: Fabricating Sustainable Shape-changing Interfaces using Soft Biopolymers. In *Proceedings of the 2024 ACM Designing Interactive Systems Conference* (IT University of Copenhagen, Denmark) *(DIS '24)*. Association for Computing Machinery, New York, NY, USA, 496–508. https://doi.org/10.1145/3643834.3661610

[71] Jifei Ou, Mélina Skouras, Nikolaos Vlavianos, Felix Heibeck, Chin-Yi Cheng, Jannik Peters, and Hiroshi Ishii. 2016. aeroMorph - Heat-sealing Inflatable Shape-change Materials for Interaction Design. In *Proceedings of the 29th Annual Symposium on User Interface Software and Technology* (Tokyo, Japan) *(UIST '16)*. Association for Computing Machinery, New York, NY, USA, 121–132. https://doi.org/10.1145/2984511.2984520

[72] Liliang Ouyang, Jason A Burdick, and Wei Sun. 2018. Facile biofabrication of heterogeneous multilayer tubular hydrogels by fast diffusion-induced gelation. *ACS applied materials & interfaces* 10, 15 (2018), 12424–12430. https://doi.org/10.1021/acsami.7b19537

[73] Jerome P Paques, Erik van der Linden, Cees JM van Rijn, and Leonard MC Sagis. 2014. Preparation methods of alginate nanoparticles. *Advances in colloid and interface science* 209 (2014), 163–171. https://doi.org/10.1016/j.cis.2014.03.009

[74] Yong-Lae Park, Bor-Rong Chen, and Robert J. Wood. 2012. Design and Fabrication of Soft Artificial Skin Using Embedded Microchannels and Liquid Conductors. *IEEE Sensors Journal* 12, 8 (2012), 2711–2718. https://doi.org/10.1109/JSEN.2012.2200790

[75] Yuecheng Peng, Danchang Yan, Haotian Chen, Yue Yang, Ye Tao, Weitao Song, Lingyun Sun, and Guanyun Wang. 2024. IntelliTex: Fabricating Low-cost and Washable Functional Textiles using A Double-coating Process. In *Proceedings of the CHI Conference on Human Factors in Computing Systems* (Honolulu, HI, USA) *(CHI '24)*. Association for Computing Machinery, New York, NY, USA, Article 859, 18 pages. https://doi.org/10.1145/3613904.3642759

[76] Uyen HT Pham, Madiha Hanif, Amit Asthana, and Samir M Iqbal. 2015. A microfluidic device approach to generate hollow alginate microfibers with controlled wall thickness and inner diameter. *Journal of Applied Physics* 117, 21 (2015), 214703. https://doi.org/10.1063/1.4919361

[77] D Quong, RJ Neufeld, G Skjåk-Bræk, and D Poncelet. 1998. External versus internal source of calcium during the gelation of alginate beads for DNA encapsulation. *Biotechnology and Bioengineering* 57, 4 (1998), 438–446. https://doi.org/10.1002/(SICI)1097-0290(19980220)57:4<438::AID-BIT7>3.0.CO;2-N

[78] Tucker Rae-Grant, Shuhong Wang, and Lining Yao. 2024. ExCell: High Expansion Ratio Moisture-Responsive Wooden Actuators for DIY Shape-Changing and Deployable Structures. In *Proceedings of the CHI Conference on Human Factors in Computing Systems* (Honolulu, HI, USA) *(CHI '24)*. Association for Computing Machinery, New York, NY, USA, Article 516, 14 pages. https://doi.org/10.1145/3613904.3642565

[79] Michael L. Rivera, S. Sandra Bae, and Scott E. Hudson. 2023. Designing a Sustainable Material for 3D Printing with Spent Coffee Grounds. In *Proceedings of the 2023 ACM Designing Interactive Systems Conference* (Pittsburgh, PA, USA) *(DIS '23)*. Association for Computing Machinery, New York, NY, USA, 294–311. https://doi.org/10.1145/3563657.3595983

[80] Michael L. Rivera, Jack Forman, Scott E. Hudson, and Lining Yao. 2020. Hydrogel-Textile Composites: Actuators for Shape-Changing Interfaces. In *Extended Abstracts of the 2020 CHI Conference on Human Factors in Computing Systems* (Honolulu, HI, USA) *(CHI EA '20)*. Association for Computing Machinery, New York, NY, USA, 1–9. https://doi.org/10.1145/3334480.3382788

[81] Cristina Rodríguez-Rivero, Loic Hilliou, Eva M Martín del Valle, and Miguel A Galán. 2014. Rheological characterization of commercial highly viscous alginate solutions in shear and extensional flows. *Rheologica acta* 53 (2014), 559–570. https://doi.org/10.1007/s00397-014-0780-4

[82] Harpreet Sareen, Udayan Umapathi, Patrick Shin, Yasuaki Kakehi, Jifei Ou, Hiroshi Ishii, and Pattie Maes. 2017. Printflatables: Printing Human-Scale, Functional and Dynamic Inflatable Objects. In *Proceedings of the 2017 CHI Conference on Human Factors in Computing Systems* (Denver, Colorado, USA) *(CHI '17)*. Association for Computing Machinery, New York, NY, USA, 3669–3680. https://doi.org/10.1145/3025453.3025898

[83] Valkyrie Savage, Ryan Schmidt, Tovi Grossman, George Fitzmaurice, and Björn Hartmann. 2014. A series of tubes: adding interactivity to 3D prints using internal pipes. In *Proceedings of the 27th Annual ACM Symposium on User Interface Software and Technology* (Honolulu, Hawaii, USA) *(UIST '14)*. Association for Computing Machinery, New York, NY, USA, 3–12. https://doi.org/10.1145/2642918.2647374

[84] Pratiksha Singh, Pankaj Baisthakur, and Omprakash S. Yemul. 2020. Synthesis, characterization and application of crosslinked alginate as green packaging material. *Heliyon* 6, 1 (2020), e03026. https://doi.org/10.1016/j.heliyon.2019.e03026

[85] Jianchun Song, Shuo Chen, Lijie Sun, Yifan Guo, Luzhi Zhang, Shuliang Wang, Huixia Xuan, Qingbao Guan, and Zhengwei You. 2020. Mechanically and Electronically Robust Transparent Organohydrogel Fibers. *Advanced Materials* 32, 8 (2020), 1906994. https://doi.org/10.1002/adma.201906994 arXiv:https://onlinelibrary.wiley.com/doi/pdf/10.1002/adma.201906994

[86] Katherine W Song, Aditi Maheshwari, Eric M Gallo, Andreea Danielescu, and Eric Paulos. 2022. Towards Decomposable Interactive Systems: Design of a Backyard-Degradable Wireless Heating Interface. In *Proceedings of the 2022 CHI Conference on Human Factors in Computing Systems* (New Orleans, LA, USA) *(CHI '22)*. Association for Computing Machinery, New York, NY, USA, Article 100, 12 pages. https://doi.org/10.1145/3491102.3502007

[87] Katherine W Song and Eric Paulos. 2021. Unmaking: Enabling and Celebrating the Creative Material of Failure, Destruction, Decay, and Deformation. In *Proceedings of the 2021 CHI Conference on Human Factors in Computing Systems* (Yokohama, Japan) *(CHI '21)*. Association for Computing Machinery, New York, NY, USA, Article 429, 12 pages. https://doi.org/10.1145/3411764.3445529

[88] Katherine Wei Song and Eric Paulos. 2023. Vim: Customizable, Decomposable Electrical Energy Storage. In *Proceedings of the 2023 CHI Conference on Human Factors in Computing Systems* (Hamburg, Germany) *(CHI '23)*. Association for Computing Machinery, New York, NY, USA, Article 180, 18 pages. https://doi.org/10.1145/3544548.3581110

[89] Paul Strohmeier, Jarrod Knibbe, Sebastian Boring, and Kasper Hornbæk. 2018. zPatch: Hybrid Resistive/Capacitive eTextile Input. In *Proceedings of the Twelfth International Conference on Tangible, Embedded, and Embodied Interaction* (Stockholm, Sweden) *(TEI '18)*. Association for Computing Machinery, New York, NY, USA, 188–198. https://doi.org/10.1145/3173225.3173242

[90] Di Sun. 2023. Sacrificial gelatin of PAM-Alginate-BC hydrogel tube with tunable diameter as nerve conduit. *Journal of Biomaterials Science, Polymer Edition* 34, 10 (2023), 1398–1407. https://doi.org/10.1080/09205063.2023.2167047

[91] Wei Sun, Yanjun Chen, Simon Zhan, Teng Han, Feng Tian, Hongan Wang, and Xing-Dong Yang. 2021. RElectrode: A Reconfigurable Electrode For Multi-Purpose Sensing Based on Microfluidics. In *Proceedings of the 2021 CHI Conference on Human Factors in Computing Systems* (Yokohama, Japan) *(CHI '21)*. Association for Computing Machinery, New York, NY, USA, Article 13, 12 pages. https://doi.org/10.1145/3411764.3445652

[92] Wenhuan Sun, Avery S Williamson, Ravesh Sukhnandan, Carmel Majidi, Lining Yao, Adam W Feinberg, and Victoria A Webster-Wood. 2023. Biodegradable, sustainable hydrogel actuators with shape and stiffness morphing capabilities via embedded 3D printing. *Advanced Functional Materials* 33, 36 (2023), 2303659. https://doi.org/10.1002/adfm.202303659

[93] Junyan Tan, Yuning Luo, Yuqiong Guo, Yue Zhou, Xinying Liao, Dingxilei Li, Xinyi Lai, and Yang Liu. 2023. Development of alginate-based hydrogels: Crosslinking strategies and biomedical applications. *International journal of biological macromolecules* 239 (2023), 124275. https://doi.org/10.1016/j.ijbiomac.2023.124275

[94] Carlos Tejada, Osamu Fujimoto, Zhiyuan Li, and Daniel Ashbrook. 2018. Blowhole: Blowing-Activated Tags for Interactive 3D-Printed Models. In *Proceedings of the 44th Graphics Interface Conference* (Toronto, Canada) *(GI '18)*. Canadian Human-Computer Communications Society, Waterloo, CAN, 131–137. https://doi.org/10.20380/GI2018.18

[95] Carlos E. Tejada, Raf Ramakers, Sebastian Boring, and Daniel Ashbrook. 2020. AirTouch: 3D-printed Touch-Sensitive Objects Using Pneumatic Sensing. In *Proceedings of the 2020 CHI Conference on Human Factors in Computing Systems*

(Honolulu, HI, USA) *(CHI '20)*. Association for Computing Machinery, New York, NY, USA, 1–10. https://doi.org/10.1145/3313831.3376136

[96] Yutaka Tokuda, Deepak Ranjan Sahoo, Matt Jones, Sriram Subramanian, and Anusha Withana. 2021. Flowcuits: Crafting Tangible and Interactive Electrical Components with Liquid Metal Circuits. In *Proceedings of the Fifteenth International Conference on Tangible, Embedded, and Embodied Interaction* (Salzburg, Austria) *(TEI '21)*. Association for Computing Machinery, New York, NY, USA, Article 35, 11 pages. https://doi.org/10.1145/3430524.3440654

[97] Ruiping Tong, Zhihui Ma, Ping Gu, Rui Yao, Tengfei Li, Mingshun Zeng, Fazhan Guo, Linfeng Liu, and Junfei Xu. 2023. Stretchable and sensitive sodium alginate ionic hydrogel fibers for flexible strain sensors. *International Journal of Biological Macromolecules* 246 (2023), 125683. https://doi.org/10.1016/j.ijbiomac.2023.125683

[98] Instructables User. n.d.. Homemade Silicone O-rings and Tubing. https://www.instructables.com/Homemade-silicone-O-rings-and-tubing/ Accessed: 2024-12-06.

[99] Eldy S. Lazaro Vasquez and Katia Vega. 2019. From plastic to biomaterials: prototyping DIY electronics with mycelium. In *Adjunct Proceedings of the 2019 ACM International Joint Conference on Pervasive and Ubiquitous Computing and Proceedings of the 2019 ACM International Symposium on Wearable Computers* (London, United Kingdom) *(UbiComp/ISWC '19 Adjunct)*. Association for Computing Machinery, New York, NY, USA, 308–311. https://doi.org/10.1145/3341162.3343808

[100] Eldy S. Lazaro Vasquez and Katia Vega. 2019. Myco-accessories: sustainable wearables with biodegradable materials. In *Proceedings of the 2019 ACM International Symposium on Wearable Computers* (London, United Kingdom) *(ISWC '19)*. Association for Computing Machinery, New York, NY, USA, 306–311. https://doi.org/10.1145/3341163.3346938

[101] Ludwig Wilhelm Wall, Alec Jacobson, Daniel Vogel, and Oliver Schneider. 2021. Scrappy: Using Scrap Material as Infill to Make Fabrication More Sustainable. In *Proceedings of the 2021 CHI Conference on Human Factors in Computing Systems* (Yokohama, Japan) *(CHI '21)*. Association for Computing Machinery, New York, NY, USA, Article 665, 12 pages. https://doi.org/10.1145/3411764.3445187

[102] Leo Q Wan, Jie Jiang, Diana E Arnold, X Edward Guo, Helen H Lu, and Van C Mow. 2008. Calcium concentration effects on the mechanical and biochemical properties of chondrocyte-alginate constructs. *Cellular and molecular bioengineering* 1 (2008), 93–102. https://doi.org/10.1007/s12195-008-0014-x

[103] Guohua Wang, Yicheng Wang, Guoqiang Lu, Shiyu Dong, Ruifen Tang, Yingying Zhao, Jun Nie, and Xiaoqun Zhu. 2024. Continuous and Controllable Preparation of Sodium Alginate Hydrogel Tubes Guided by the Soft Cap Inspired by the Apical Growth of the Plant. *ACS Applied Materials & Interfaces* 16, 23 (2024), 29600–29609. https://doi.org/10.1021/acsami.4c00655 arXiv:https://doi.org/10.1021/acsami.4c00655 PMID: 38832656.

[104] Guanyun Wang, Kuangqi Zhu, Lingchuan Zhou, Mengyan Guo, Haotian Chen, Zihan Yan, Deying Pan, Yue Yang, Jiaji Li, Jiang Wu, Ye Tao, and Lingyun Sun. 2023. PneuFab: Designing Low-Cost 3D-Printed Inflatable Structures for Blow Molding Artifacts. In *Proceedings of the 2023 CHI Conference on Human Factors in Computing Systems* (Hamburg, Germany) *(CHI '23)*. Association for Computing Machinery, New York, NY, USA, Article 693, 17 pages. https://doi.org/10.1145/3544548.3580923

[105] Jennifer Weiler, Piyum Fernando, Nipuni Siyambalapitiya, and Stacey Kuznetsov. 2019. Mycelium Artifacts: Exploring Shapeable and Accessible Biofabrication. In *Companion Publication of the 2019 on Designing Interactive Systems Conference 2019 Companion* (San Diego, CA, USA) *(DIS '19 Companion)*. Association for Computing Machinery, New York, NY, USA, 69–72. https://doi.org/10.1145/3301019.3325156

[106] Baoyi Wu, Yukun Jian, Xiaoxia Le, Han Lin, Shuxin Wei, Wei Lu, Jiawei Zhang, Afang Zhang, Chih-Feng Huang, and Tao Chen. 2019. Supramolecular fabrication of complex 3D hollow polymeric hydrogels with shape and function diversity. *ACS applied materials & interfaces* 11, 51 (2019), 48564–48573. https://doi.org/10.1021/acsami.9b17440

[107] Di Wu, Emily Guan, Yunjia Zhang, Hsuanju Lai, Qiuyu Lu, and Lining Yao. 2024. Waxpaper Actuator: Sequentially and Conditionally Programmable Wax Paper for Morphing Interfaces. In *Proceedings of the CHI Conference on Human Factors in Computing Systems* (Honolulu, HI, USA) *(CHI '24)*. Association for Computing Machinery, New York, NY, USA, Article 865, 16 pages. https://doi.org/10.1145/3613904.3642373

[108] Shanel Wu and Laura Devendorf. 2020. Unfabricate: Designing Smart Textiles for Disassembly. In *Proceedings of the 2020 CHI Conference on Human Factors in Computing Systems* (Honolulu, HI, USA) *(CHI '20)*. Association for Computing Machinery, New York, NY, USA, 1–14. https://doi.org/10.1145/3313831.3376227

[109] Ruoxiao Xie, Peidi Xu, Yupeng Liu, Lili Li, Guoan Luo, Mingyu Ding, and Qionglin Liang. 2018. Necklace-like microfibers with variable knots and perfusable channels fabricated by an oil-free microfluidic spinning process. *Advanced Materials* 30, 14 (2018), 1705082. https://doi.org/10.1002/adma.201705082

[110] Junichi Yamaoka, Ryuma Niiyama, and Yasuaki Kakehi. 2017. BlowFab: Rapid Prototyping for Rigid and Reusable Objects using Inflation of Laser-cut Surfaces. In *Proceedings of the 30th Annual ACM Symposium on User Interface Software and Technology* (Québec City, QC, Canada) *(UIST '17)*. Association for Computing Machinery, New York, NY, USA, 461–469. https://doi.org/10.1145/3126594.3126624

[111] Zeyu Yan and Huaishu Peng. 2021. FabHydro: Printing Interactive Hydraulic Devices with an Affordable SLA 3D Printer. In *The 34th Annual ACM Symposium on User Interface Software and Technology* (Virtual Event, USA) *(UIST '21)*. Association for Computing Machinery, New York, NY, USA, 298–311. https://doi.org/10.1145/3472749.3474751

[112] Humphrey Yang, Danli Luo, Kuanren Qian, and Lining Yao. 2021. Freeform Fabrication of Fluidic Edible Materials. In *Proceedings of the 2021 CHI Conference on Human Factors in Computing Systems* (Yokohama, Japan) *(CHI '21)*. Association for Computing Machinery, New York, NY, USA, Article 620, 10 pages. https://doi.org/10.1145/3411764.3445097

[113] Yue Yang, Lei Ren, Chuang Chen, Bin Hu, Zhuoyi Zhang, Xinyan Li, Yanchen Shen, Kuangqi Zhu, Junzhe Ji, Yuyang Zhang, Yongbo Ni, Jiayi Wu, Qi Wang, Jiang Wu, Lingyun Sun, Ye Tao, and Guanyun Wang. 2024. SnapInflatables: Designing Inflatables with Snap-through Instability for Responsive Interaction. In *Proceedings of the CHI Conference on Human Factors in Computing Systems* (Honolulu, HI, USA) *(CHI '24)*. Association for Computing Machinery, New York, NY, USA, Article 342, 15 pages. https://doi.org/10.1145/3613904.3642933

[114] Lining Yao, Ryuma Niiyama, Jifei Ou, Sean Follmer, Clark Della Silva, and Hiroshi Ishii. 2013. PneUI: pneumatically actuated soft composite materials for shape changing interfaces. In *Proceedings of the 26th Annual ACM Symposium on User Interface Software and Technology* (St. Andrews, Scotland, United Kingdom) *(UIST '13)*. Association for Computing Machinery, New York, NY, USA, 13–22. https://doi.org/10.1145/2501988.2502037

[115] Seung Mi Yoo and Raja Ghosh. 2014. Fabrication of alginate fibers using a microporous membrane based molding technique. *Biochemical Engineering Journal* 91 (2014), 58–65. https://doi.org/10.1016/j.bej.2014.07.006

[116] Tianyu Yu, Weiye Xu, Haiqing Xu, Guanhong Liu, Chang Liu, Guanyun Wang, and Haipeng Mi. 2023. Thermotion: Design and Fabrication of Thermofluidic Composites for Animation Effects on Object Surfaces. In *Proceedings of the 2023 CHI Conference on Human Factors in Computing Systems* (Hamburg, Germany) *(CHI '23)*. Association for Computing Machinery, New York, NY, USA, Article 425, 19 pages. https://doi.org/10.1145/3544548.3580743

[117] Yunru Yu, Fanfan Fu, Luoran Shang, Yao Cheng, Zhongze Gu, and Yuanjin Zhao. 2017. Bioinspired helical microfibers from microfluidics. *Advanced Materials* 29, 18 (2017), 1605765. https://doi.org/10.1002/adma.201605765

[118] Hyunwoo Yuk, Shaoting Lin, Chu Ma, Mahdi Takaffoli, Nicolas X Fang, and Xuanhe Zhao. 2017. Hydraulic hydrogel actuators and robots optically and sonically camouflaged in water. *Nature communications* 8, 1 (2017), 14230. https://doi.org/10.1038/ncomms14230

[119] Guoxu Zhao, Tinglong Wu, Ruhai Wang, Zhong Li, Qingzhen Yang, Lei Wang, Hongwei Zhou, Birui Jin, Hao Liu, Yunsheng Fang, et al. 2023. Hydrogel-assisted microfluidic spinning of stretchable fibers via fluidic and interfacial self-adaptations. *Science Advances* 9, 42 (2023), eadj5407. https://doi.org/10.1126/sciadv.adj5407

[120] Hongli Zhu, Heming Wang, Yuanyuan Li, Wenzhong Bao, Zhiqiang Fang, Colin Preston, Oeyvind Vaaland, Zhiyong Ren, and Liangbing Hu. 2014. Lightweight, conductive hollow fibers from nature as sustainable electrode materials for microbial energy harvesting. *Nano Energy* 10 (2014), 268–276. https://doi.org/10.1016/j.nanoen.2014.08.014

[121] Jingwen Zhu, Lily Winagle, and Hsin-Liu (Cindy) Kao. 2024. EcoThreads: Prototyping Biodegradable E-textiles Through Thread-based Fabrication. In *Proceedings of the 2024 CHI Conference on Human Factors in Computing Systems* (Honolulu, HI, USA) *(CHI '24)*. Association for Computing Machinery, New York, NY, USA, Article 857, 17 pages. https://doi.org/10.1145/3613904.3642718

[122] Yujuan Zhu, Li Wang, Fangchao Yin, Yue Yu, Yaqing Wang, Hui Liu, Hui Wang, Ning Sun, Haitao Liu, and Jianhua Qin. 2017. A hollow fiber system for simple generation of human brain organoids. *Integrative biology* 9, 9 (2017), 774–781. https://doi.org/10.1039/C7IB00080D

[123] GONG Zongqiang, Li Peijun, BM Wilke, and Kassem Alef. 2008. Effects of vegetable oil residue after soil extraction on physical-chemical properties of sandy soil and plant growth. *Journal of Environmental Sciences* 20, 12 (2008), 1458–1462. https://doi.org/10.1016/S1001-0742(08)62549-8